

NASA Technical Memorandum 88866

Finite Element Analysis of Electromagnetic Propagation in an Absorbing Wave Guide

(NASA-TM-88866) FINITE ELEMENT ANALYSIS OF
ELECTROMAGNETIC PROPAGATION IN AN ABSORBING
WAVE GUIDE (NASA) 54 P CSCL 20C

N87-18391

Unclas
G3/70 43273

Kenneth J. Baumeister
Lewis Research Center
Cleveland, Ohio

Prepared for the
1986 Winter Annual Meeting of the
American Society of Mechanical Engineers
Anaheim, California, December 7-12, 1986

NASA

FINITE ELEMENT ANALYSIS OF ELECTROMAGNETIC PROPAGATION
IN AN ABSORBING WAVE GUIDE

Kenneth J. Baumeister
National Aeronautics and Space Administration
Lewis Research Center
Cleveland, Ohio 44135

SUMMARY

Wave guides play a significant role in microwave space communication systems. The attenuation per unit length of the guide depends on its construction and design frequency range. A finite element Galerkin formulation has been developed to study TM electromagnetic propagation in complex two-dimensional absorbing wave guides. The analysis models the electromagnetic absorptive characteristics of a general wave guide which could be used to determine wall losses or simulate resistive terminations fitted into the ends of a guide. It is believed that the general conclusions drawn by using this simpler two-dimensional geometry will be fundamentally the same for other geometries.

In formulating the finite element solution, the continuous electromagnetic field is divided into a number of triangular discrete areas staked out by nodal points which are spread through out the field. The nodal points can be placed at any position desired. Thus, the finite element formulation can readily handle geometrical complications such as axial and transverse variations in wall properties as well as cross-sectional area variations. The governing electromagnetic finite element equations and the appropriate boundary conditions are presented for a finite duct with known incident modes. The entrance and exit boundary conditions are developed by coupling the finite element solutions to the eigen functions of an infinite uniform perfect conducting duct. Example solutions are presented for electromagnetic propagation with perfect conducting and absorbing duct walls.

INTRODUCTION

Wave guides play a significant role in microwave space communication systems. Depending on the material properties of the wave guide and its design frequency range, the guide will attenuate a signal transmitted in the guide (ref. 1, p. 295). In general, losses in wave guides are undesirable; however, in power measurement applications, electromagnetic wave guides are sometimes fitted with fixed resistive terminations, movable vane or flop attenuators (ref. 1, p. 326) to absorb radiation and reduce reflections. To better understand the microwave absorption process, in the present paper a finite element Galerkin formulation has been developed to study the power absorption characteristics of an electromagnetic wave guide.

The numerical program to be presented herein is complimented by Grant effort at Ohio State University, the University of Illinois, and Northwestern University. The work at Ohio State and Illinois is primarily analytical in nature (ref. 2) while the research at Northwestern employs the transient finite difference technique (refs. 3 and 4). In addition, Rice (ref. 5) at NASA Lewis is developing simple analytical correlation for electronic properties which

produce the highest possible attenuation for a single mode in an infinitely long duct. Such an analysis is extremely useful for a numerical program, since the analysis gives a reasonable estimate of the electrical properties which will produce significant attenuation.

The finite element solution developed herein models the variable property Helmholtz equation in a rectangular two-dimensional wave guide with complex structural wall boundary conditions and multiple mode inputs. In the finite element solution, the continuous electromagnetic field is divided into a number of triangular discrete areas staked out by nodal points which are spread throughout the field. Since the nodal points can be placed at any position desired, the finite element formulation can readily handle geometrical complications such as axial variations in wall properties as well as cross-sectional area variations. This finite element solution bypasses the conventional eigenvalue problem with its associated modes which have been considered in earlier works on electromagnetic propagation in ducts (ref. 6, p. 88).

The inlet and exit boundary conditions associated with the finite element analysis of electromagnetic propagation must be flexible enough to account for reflection of energy which can occur from wall changes inside the guide or from abrupt exit terminations. The appropriate boundary conditions are similar to those associated with flow gust disturbances, duct acoustics (ref. 7), and thermal wave propagation (ref. 8). These problems occur in unsteady aerodynamics. An additional motivation for the present study is the continuing interest at NASA Lewis in numerical modeling of unsteady aerodynamics and general wave propagation in ducts.

In setting up the inlet and exit boundary conditions, the variable property absorbing portion of the wave guide is assumed to be joined by uniform, infinitely long, and perfectly conducting entrance and exit ports. In the entrance port, a known source of electromagnetic energy is assumed to be incident on the complex absorbing region which is to be modeled by the finite element analysis. For a single dominant input mode, Silvester, and Ferrar (ref. 6, p. 177) developed some mathematical constraints for the entrance and exit conditions. For this paper, however, the entrance and exit boundary conditions are developed for multimode propagation by coupling the finite element solutions to the complete set of eigen functions of a uniform conducting duct. In acoustics, numerical calculations using this boundary constraint were found to be in excellent agreement with experimental results (ref. 9).

First, the governing electromagnetic equation and the appropriate boundary conditions are presented. Next, the finite element modeling is presented. Immediately following the mathematical development, numerical validation examples are presented and compared with known analytical results. Finally, the last set of example problems treat electromagnetic propagation with an absorbing boundary.

NOMENCLATURE

A_n^+	mode amplitude of plus going entrance waves, equation (29)
A_n^-	mode amplitude of reflected negative going entrance waves, equation (29)

B	magnetic flux density
B_n^+	mode amplitude of plus going exit waves, equation (33)
B_{0n}^+	modified mode amplitude of plus going exit waves, equation (52)
b'	characteristic duct height
b_a	dimensionless entrance height b_a'/b'
b_b	dimensionless exit height b_b'/b'
c_0'	speed of light in vacuum
$\bar{E}_t(x,y,z,t)$	electric field, equation (6)
\bar{E}	harmonic electric field vector, $E(x,y,z)$
e_x, e_y, e_z	unit vectors in coordinate directions
F	right hand side, equation (80)
f	dimensionless frequency, equation (9)
$\bar{H}_t(x,y,z,t)$	magnetic intensity, equation (6)
\bar{H}	harmonic magnetic intensity vector, $H(x,y,z)$, equation (8)
H_x	x component of magnetic intensity
H_{i0}	magnitude of incident magnetic intensity, equation (92).
H_{xi}	incident magnetic intensity, equation (91)
H_{xr}	reflected magnetic intensity, equation (91)
H_{r0}	magnitude of reflected magnetic intensity, equation (93)
H_{xt}	transmitted magnetic intensity, equation (94)
H_{t0}	magnitude of transmitted magnetic intensity, equation (94)
$ H_{x\max} $	maximum value of magnitude of magnetic intensity in plotting domain, equation (106)
$ H_{x\min} $	minimum value of magnitude of magnetic intensity in plotting domain, equation (106)
H_0'	normalizing magnitude of magnetic intensity
\tilde{H}_x	finite element approximation to H_x
I	total number of line increments, equation (46)
Im	imaginary part

j	$\sqrt{-1}$
$[K]$	global stiffness matrix, equation (80)
$[K]^e$	element stiffness matrix, equation (76)
$K_{1,j}^{(e)}$	element stiffness coefficient, equation (77)
k	wave number, equation (28)
k_{zn}	axial modal wave number, equation (30)
k_e	element modal wave number, equation (78)
L	dimensionless length, L'/b'
L_d	position of material change, see equation (99)
M	number of elements
m	mode number, equation (48)
N	number of nodes
N_m	number of modes
N_1, N_2, N_3	local interpolation shape functions
n	mode number, equation (29)
\bar{n}	outward normal unit vector
P_{ave}	Poynting vectors, equation (87)
P_T	total power transferred, equation (88)
R	residual error, equation (60)
Re	real part
S	length of line segment on boundary
t	dimensionless time, equation (5)
V	vector quantity, equation (64)
W_i	weight, equation (58)
x	dimensionless transverse distance, x'/b' , equation (7)
y	dimensionless transverse distance, y'/b' , equation (7)
z	dimensionless axial distance, z'/b' , equation (7)
α	damping coefficient, equation (96)

β	propagation coefficient, equation (96)
Γ	reflection coefficient, equation (101)
γ	complex propagation constant, equation (92)
ϵ	dielectric constant, ϵ'/ϵ_0'
ϵ_a	permittivity in entrance duct
ϵ'	permittivity
ϵ_0'	permittivity in vacuum
ϵ_c	conductance permittivity, equation (12)
ϵ_T	total permittivity, equation (12)
η	impedance, equation (13)
μ	permeability, μ'/μ_0'
μ'	dimensional permeability
μ_0'	permeability in vacuum
σ	conductance, equation (7)
τ	transmission coefficients, equation (102)
Φ	global unknown vector, equation (79)
ψ	scalar, equation (62)
ω	angular velocity, equation (9)

Subscripts

x,y,z scalar vector components

Superscripts

(1) region 1
 (2) region 2
 * complex conjugation
 ' dimensional quantity
 T transpose
 () vector quantity

GOVERNING EQUATION - AND MODEL

Basic Model

Consider an electromagnetic wave propagating from a transmitting antenna and incident on a two-dimensional wave guide as shown in figure 1. As the wave encounters the inlet, energy will be diffracted from the lip and redirected into space, while some energy will couple to the duct modes and be transmitted into the guide. Inside the guide, diffraction, absorption, and reflection will occur at variable property absorbing regions. Finally, energy will be transmitted down the duct and some will be reflected back out the inlet.

The present paper will focus on the interaction of propagating duct modes with the wall as shown in figure 2. The model is composed of three regions. In the uniform, infinitely long and perfectly conducting entrance and exit regions, the exact solution of the governing differential equations can be easily written in terms of the duct modes. In the absorbing variable property region of figure 2, the finite element analysis is employed to determine the field in the variable property nonuniform regions. As previously discussed, the transmitting antenna, (see fig. 1), sends electromagnetic waves into the guide which are either reflected, absorbed, or transmitted in the absorbing region. Electromagnetic mode reflection at the inlet to the duct absorbing region and the transmission at the outlet of the absorbing region are modeled by matching the finite element solution in the interior of the nonuniformity to analytical eigenfunctions expansions in the uniform inlet and outlet ducts. This permits a multimodal representation accounting for reflection and mode conversion by the nonuniformity (ref. 9).

MAXWELL'S EQUATION

The governing differential equations describing the propagation of electromagnetic energy are the two Maxwell's equations.

$$\nabla' \times \bar{E}'_t(x', y', z', t') = - \frac{\partial}{\partial t'} \mu' \bar{H}'_t(x', y', z', t') \quad (1)$$

$$\nabla' \times \bar{H}'_t(x', y', z', t') = \sigma' E'_t(x', y', z', t') + \frac{\partial}{\partial t'} \epsilon' \bar{E}'_t(x', y', z', t') \quad (2)$$

In the foregoing equations, the prime, ', is used to denote a dimensional quantity. These and all other symbols used in the report are defined in the Nomenclature. Vector equations (1) and (2) represent six scalar equations needed to determine the six unknowns scalars $E'_{tx}(x', y', z', t')$,

$E'_{ty}(x', y', z', t')$, $E'_{tz}(x', y', z', t')$, $H'_{tx}(x', y', z', t')$, $H'_{ty}(x', y', z', t')$, and $H'_{tz}(x', y', z', t')$. The subscript t indicates time dependent fields.

Later, when the assumption of harmonic time dependence is assumed, the subscript t will be dropped.

The nondimensionalization begins with the dimensionless magnetic field $H'_t(x', y', z', t')$, permittivity ϵ' , permeability μ' , and electric field $E'_t(x', y', z', t')$ and introduces their nondimensional equivalents (no primes).

The scaling factors are the entrance duct height b' , permittivity of a vacuum ϵ'_0 , permeability of a vacuum μ'_0 , velocity of light in a vacuum c'_0 , and some magnitude of magnetic intensity H'_0 . Using these parameters, the dimensionless Maxwell's equations become

$$\nabla \times \bar{E}_t(x, y, z, t) = -\frac{\partial}{\partial t} \mu \bar{H}_t(x, y, z, t) \quad (3)$$

$$\nabla \times \bar{H}_t(x, y, z, t) = \sigma \bar{E}_t(x, y, z, t) + \frac{\partial}{\partial t} \epsilon \bar{E}_t(x, y, z, t) \quad (4)$$

where ϵ is the dielectric constant with the following dimensionless quantitative defined:

$$t = \frac{c'_0}{b'} t' \quad c'_0 = 1 / \sqrt{\mu'_0 \epsilon'_0} \quad (5)$$

$$\bar{H}_t(x, y, z, t) = \frac{\bar{H}'(x', y', z', t')}{H'_0} \quad \bar{E}_t(x, y, z, t) = \sqrt{\frac{\epsilon'_0}{\mu'_0}} \frac{E'(x', y', z', t')}{H'_0} \quad (6)$$

$$\sigma = \frac{\sigma' b'}{\epsilon'_0 c'_0} \quad x = \frac{x'}{b'} \quad y = \frac{y'}{b'} \quad z = \frac{z'}{b'} \quad (7)$$

As a further simplification, for harmonic steady state analysis it is usually assumed

$$\bar{H}_t(x, y, z, t) = \bar{H}(x, y, z) e^{+j\omega' t'} = \bar{H}(x, y, z) e^{+j\omega t} \quad (8)$$

where the dimensionless frequency is defined

$$f = \frac{f' b'}{c'_0} \quad \omega = \frac{\omega' b'}{c'_0} \quad \omega = 2\pi f \quad (9)$$

Similar assumptions for E are also employed. Substituting equations (8) and (9) into equations (3) and (4) yields

$$\nabla \times \bar{E} = -j\omega \mu \bar{H} \quad (10)$$

$$\nabla \times \bar{H} = j\omega \epsilon_T \bar{E} \quad (11)$$

where the total permittivity includes conduction

$$\epsilon_T = \epsilon - j\epsilon_c \quad (12)$$

$$\epsilon_c = \frac{\sigma}{\omega} = \frac{\sigma'}{\omega' \epsilon'_0} \quad (13)$$

The magnetic and electric fields are now considered to be harmonic spatially dependent variables.

NONHOMOGENEOUS VARIABLE PROPERTY WAVE EQUATION

The number of dependent variables can be reduced by combining Maxwell's equations (10) and (11) into a single wave equation. This operation will lead to a 50 percent reduction of computer storage requirements. It is also desirable to develop a wave equation that could be used for varying media properties so that no special treatment of the interface between materials is required. That is, the same equations apply in the duct and in the absorber region and only the material properties are changed.

Rewriting equation (11),

$$\frac{\nabla \times \bar{H}}{j\omega \epsilon_T} = \bar{E} \quad (14)$$

and taking the curl

$$\nabla \times \left[\frac{\nabla \times \bar{H}}{j\omega \epsilon_T} \right] = \nabla \times \bar{E} \quad (15)$$

The constants $j\omega$ are independent of space and can be pulled out the curl operator in equation (15); however, ϵ_T must remain inside since ϵ_T is now assumed a function of the spatial dimensions.

$$\frac{1}{j\omega} \nabla \times \left[\frac{\nabla \times \bar{H}}{\epsilon_T} \right] = \nabla \times \bar{E} \quad (16)$$

Substituting equation (16) into equation (10) yields our nonhomogenous governing wave equation.

$$\nabla \times \left[\frac{\nabla \times \bar{H}}{\epsilon_T} \right] = \omega^2 \mu \bar{H} \quad (17)$$

TM VARIABLE PROPERTY 2D WAVE EQUATION

As customary in electromagnetics as well as fluid mechanics and heat transfer (ref. 10), simple inlet profiles of the dependent variable are commonly assumed. Herein, transverse magnetic (TM) waves will be assumed to represent the input electromagnetic modes propagating down the entrance duct towards the nonuniform variable property section of the duct. The assumption is made that only one component of the \bar{H} vector will exist in the problem domain, that is,

$$\bar{H}(y, z) = H_x(y, z) \mathbf{e}_x \quad (18)$$

where \mathbf{e}_x is a unit vector in the x direction (into the paper as shown in fig. 3). The magnitude of the single x component of the vector \bar{H} depends only on the two spatial dimensions y and z . The question remains, however, would a z component of the magnetic field be generated in the the variable property region.

The validity of assumption (18) can be verified by consideration of the magnetic source equation (divergence equation);

$$\nabla \cdot \vec{B} = 0 \quad (19)$$

where B is the magnetic flux density, a vector quantity defined by

$$B_x = \mu(y,z)H_x \quad (20)$$

Recall, the above equation can be derived directly from Maxwell's first two equations (ref. 7, p. 280). Combining equations (19) and (20) and using the usual vector identities (ref. 7, p. 578) equation 19 can be rewritten as

$$\mu(y,z)\nabla \cdot \vec{H} + \vec{H} \cdot \nabla\mu(y,z) = 0 \quad (21)$$

Substituting in equation (18) into equation (21) yields

$$\mu \frac{\partial}{\partial x} [H_x(y,z)] + H_x(y,z) e_x \cdot \left[\frac{\partial \mu}{\partial y} e_y + \frac{\partial \mu}{\partial z} e_z \right] = 0 \quad (22)$$

Since all the terms on the left hand side of equation (22) are identical to zero, equation (18) is a valid solution to the problem, independent of property and geometry changes.

Using equation (18) to evaluate the term in brackets in equation (17) yields

$$\frac{\nabla \times H}{\epsilon_T} = \frac{1}{\epsilon_T} \frac{\partial H_x}{\partial z} e_y - \frac{\partial H_x}{\partial y} e_z \quad (23)$$

Next, the complete expression for the left hand side of equation (17) is determined by taking the curl of equation (23), as follows,

$$\nabla \times \left[\frac{\nabla \times H}{\epsilon_T} \right] = \left[\frac{\partial}{\partial y} \left(-\frac{1}{\epsilon_T} \frac{\partial H_x}{\partial y} \right) + \frac{\partial}{\partial z} \left(-\frac{1}{\epsilon_T} \frac{\partial H_x}{\partial z} \right) \right] e_x \quad (24)$$

Finally, substituting equation (24) for the left hand side of equation (17) yields the scalar wave equation,

$$\frac{\partial}{\partial y} \left(\frac{1}{\epsilon_T} \frac{\partial H_x}{\partial y} \right) + \frac{\partial}{\partial z} \left(\frac{1}{\epsilon_T} \frac{\partial H_x}{\partial z} \right) + \omega^2 \mu H_x = 0 \quad (25)$$

In vector form,

$$\nabla \cdot \frac{1}{\epsilon_T} \nabla H_x + \omega^2 \mu H_x = 0 \quad (26)$$

Equation (26) represents the governing wave equation to be solved by finite element theory.

UNIFORM DUCT ANALYTICAL SOLUTIONS

The analytical solutions of equation (26) for wave propagation in the uniform perfect conducting inlet and exit ports will be employed to give the proper termination boundary conditions for the finite element region. The analytical solution for TM waves traveling between parallel plates is standard textbook material (ref. 11, p. 458) and quite simple in form. Consequently, these solutions will now be presented before the complete discussion of boundary conditions associated with the finite element solution in the variable property region.

In the entrance and exit regions, the medium properties are assumed constant and real ($\sigma = 0$) such that the wave equation (26) reduces to

$$\nabla^2 H_x + k^2 H_x = 0 \quad (27)$$

where the free medium wave number k equals

$$k = \omega \sqrt{\mu \epsilon} \quad (28)$$

In the analytical entrance region, the eigen value solution of equation (27) yields (ref. 11, p. 458) for the coordinate system shown in figure 3.

$$H_{xa} = \sum_{n=1}^{N_m} A_n^+ \cos\left(\frac{(n-1)\pi}{b_a} y\right) e^{-jk_{zn}z} + \sum_{n=1}^{N_m} A_n^- \cos\left(\frac{(n-1)\pi}{b_a} y\right) e^{+jk_{zn}z} \quad (29)$$

For the $e^{j\omega t}$ time dependence used here, equation (8), the $A_n^+ e^{-jk_{zn}z}$ term represents a wave propagating in the positive z direction while the $A_n^- e^{+jk_{zn}z}$ represent a wave moving in the negative z direction (exactly opposite would occur had a $e^{-j\omega t}$ time dependence been assumed, see reference 11, p. 308).

The axial wave number k_{zn} in equation (29) is

$$k_{zn} = +k \sqrt{1 - \left(\frac{(n-1)\pi}{b_a k}\right)^2} \quad \left(\frac{n\pi}{b_a k}\right) \leq 1 \quad (30)$$

$$k_{zn} = -jk \left| \sqrt{\left(\frac{(n-1)\pi}{b_a k}\right)^2 - 1} \right| \quad \left(\frac{n\pi}{b_a k}\right) > 1 \quad (31)$$

Equation (31) represents the condition where the mode is cut-off (nonpropagating). The negative sign is chosen to produce mode decay in the positive direction for the A^+ modes and mode decay in the negative direction for the A^- modes. Since the characteristic duct height b' will be set equal to the entrance duct height, b_a will have a numerical value of unity.

The modal expression represented by equation (29) has been transacted to a total of N_m modes of the infinite number possible. Thus, a total of

N_m unknown modal amplitudes $A_1^-, A_2^-, \dots, A_{N_m}^-$ have been introduced. N_m constraint equations will be required to determine each of these unknown reflection coefficients. The equations used to define these coefficients will be introduced in the following section on boundary conditions.

The gradient of H_x in the axial direction will play a major role in the finite element solution to be presented. The gradient is written as

$$\begin{aligned} \frac{\partial H_{xa}}{\partial z} = & \sum_{n=1}^{N_m} -jA_n^+ k_{zn} \cos\left(\frac{(n-1)\pi}{b_a} y\right) e^{-jk_{zn}z} \\ & + \sum_{n=1}^{N_m} jA_n^- k_{zn} \cos\left(\frac{(n-1)\pi}{b_a} y\right) e^{+jk_{zn}z} \end{aligned} \quad (32)$$

Finally, in the exit port, a similar solution of the following form exits

$$H_{xb} = \sum_{n=1}^{N_m} B_n^+ \cos\left(\frac{(n-1)\pi}{b_b} y\right) e^{-jk_{zn}z} \quad (33)$$

and

$$\frac{\partial H_{xb}}{\partial z} = \sum_{n=1}^{N_m} -jB_n^+ k_{zn} \cos\left(\frac{(n-1)\pi}{b_b} y\right) e^{-jk_{zn}z} \quad (34)$$

Here, only positive going waves are assumed and the eigenfunctions and wave number are expressed in the height of the exit duct b_b .

BOUNDARY CONDITIONS

A variety of boundary condition will be used in the finite element solution of equation (26) for the model problem which is displayed in schematic form in figure 2. Each of the required conditions will now be briefly discussed.

Input Condition

The analysis assumes a given number of propagating (see eq. (30)) A_n^+ modes. These modes effectively set the level of the magnetic field in the finite element region and can be viewed as the equivalent Dirichlet boundary conditions required for elliptic boundary value problem as defined by equation (26).

Perfect Conducting Wall Conditions

At a perfect conducting wall, the tangential component of the electric field vector is zero (ref. 11, eq. 7-52a or ref. 12, eq. 1.69)

$$E_t = 0 \quad (35)$$

Thus, for example,

$$E_x = E_z = 0 \quad (36)$$

Along any of the horizontal perfectly conducting surfaces of figure 2. Since, the H_x equation (26) has been program for solution, the relationship between E_z given by equation (35) and H_x at the boundary must be developed. In particular, the finite element analysis well require information on the gradient of H_x at a perfect conducting boundary.

From equation (14), the E_z component of Maxwell equation can be written as (ref. 13, eqs. (1) to (4)).

$$E_z = \frac{1}{j\omega\epsilon_T} \left[\frac{\partial H_y}{\partial x} - \frac{\partial H_x}{\partial y} \right] \quad (37)$$

or since $H_y = 0$

$$E_z = - \frac{1}{j\omega\epsilon_T} \frac{\partial H_x}{\partial y} \quad (38)$$

Since E_z is zero at perfect conducting horizontal boundary

$$\frac{\partial H_x}{\partial y} = 0 \quad (39)$$

Now, since the finite element analysis will require information about ∇H_x at its boundary, let us expand at the upper horizontal boundary.

$$\nabla H_x \cdot n = \nabla H_x \cdot e_y = \left(\frac{\partial H_x}{\partial x} e_x + \frac{\partial H_x}{\partial y} e_y + \frac{\partial H_x}{\partial z} e_z \right) \cdot e_y \quad (40)$$

Since only the dot product $e_y \cdot e_y$ gives a contribution,

$$\nabla H_x \cdot \bar{n} = \frac{\partial H_x}{\partial y} \quad (41)$$

Since the electric field tangency condition for this problem requires $\partial H_x / \partial y$ is zero (eq. (39))

$$\nabla H_x \cdot \bar{n} = 0 \quad (42)$$

at the upper horizontal surface. It is easily shown that this condition applies to all perfect conducting surfaces no matter their spatial orientation.

Continuity at Inlet and Exit

In general, the tangential component of an H field is continuous across an interface (ref. 12, eq. (1.61)) except at perfect conductor where a surface current exists (ref. 11, eqs. 7-52(b)). Thus, the boundary condition becomes

$$H_{1t} = H_{2t} \quad (43)$$

or the tangential components are H_x

$$H_{xa} = \tilde{H}_x \quad (z = 0; 0 < y < b_a) \quad (44)$$

where H_{xa} is the modal representation of magnetic field in the analytical inlet region given by equation (29) and \tilde{H}_x represent the finite element approximation for H_x at the interface. The hat over \tilde{H}_x implies an approximate finite element numerical solution to be discussed in detail in a following section.

At the inlet interface, shown by the dashed line in figure 2, the H_{xa} in the analytical region given by equation (29) must match the magnetic field defined by the finite element nodal points along the boundary interface. Many possible matching methods can be employed for this boundary condition, such as point collocation, least squares or weighted residuals. A weighted residual approach was used herein with the weighting function equal to the eigenfunctions

$$\int_0^{b_a} [H_{xa}(y) - \tilde{H}(y)] \cos\left(\frac{(m-1)\pi y}{b_a}\right) dy \Big|_{z=0} = 0$$

$$(N_m \text{ equations, } m = 1, 2, 3, \dots, N_m) \quad (45)$$

Equation (45) represents N_m separate equations; one for each coefficient defined in equation (29).

For a particular weighting function $\cos((m-1)\pi y/b_a)$, a very simple numerical approximation for the line integral can be written as

$$\sum_{i=1}^I [H_{xa}(y_i) - H_i] \cos\left(\frac{(m-1)\pi y_i}{b_a}\right) \Delta y_i = 0 \quad (z = 0)$$

$$(N_m \text{ equation, } m = 1, 2, 3, \dots, N_m) \quad (46)$$

where the Δy_i is defined as shown in figure 4. Substituting in the value of H_{xa} from equation (29) yields, moving known A+ coefficients to right hand side,

$$\sum_{i=1}^I \Delta y_i \left[\cos \left(\frac{(m-1)\pi y_i}{b_a} \right) \left\{ \sum_{n=1}^{N_m} A_n^- \cos \left(\frac{(n-1)\pi}{b_a} y_i \right) - H_i \right\} \right]$$

$$= - \sum_{i=1}^I \Delta y_i \cos \left(\frac{(m-1)\pi y_i}{b_a} \right) \sum_{n=1}^{N_m} A_n^+ \cos \left(\frac{(n-1)\pi y_i}{b_a} \right) \quad (z=0)$$

(N_m equations, m = 1, 2, . . . N_m) (47)

where the mth equation is defined by the first cosine term on both sides of equation (47). In slightly different form

$$\sum_{n=1}^{N_m} \left[A_n^- \sum_{i=1}^I \cos \left(\frac{(n-1)\pi}{b_a} y_i \right) \cos \left(\frac{(m-1)\pi}{b_a} \Delta y_i \right) \Delta y_i \right] - \sum_{i=1}^I H_i \cos \left(\frac{(m-1)\pi}{b_a} y_i \right) \Delta y_i =$$

$$- \sum_{n=1}^{N_m} A_n^+ \left[\sum_{i=1}^I \cos \left(\frac{(n-1)\pi}{b_a} y_i \right) \cos \left(\frac{(m-1)\pi}{b_a} y_i \right) \Delta y_i \right] \quad (z=0)$$

(N_m separate equations. m = 1, 2, . . . N_m) (48)

The terms on the right side represent the known forcing functions to the equation since all the values of A_n⁺ are assumed known. The left hand side contains the N_m unknown reflection coefficients and the unknown nodal values of H_i at the finite element grid. Recall the modal equation used to specify the oncoming and reflected field was truncated to contain N_m unknown reflection coefficients A₁⁻, A₂⁻, A₃⁻, . . . A_{N_m}⁻. Equation (48) represents one of the N_m scalar equations required to determine all A_n⁻ reflective coefficients. At the exit, equation (45) becomes

$$\int_0^{b_b} \left[H_{xb}(y) - \tilde{H}(y) \right] \cos \left(\frac{(m-1)\pi y}{b_b} \right) dy \Big|_{z=L} = 0$$

(N_m equations, m = 1, 2, 3, . . . N_m) (49)

or in terms of the modes

$$\sum_{n=1}^{N_m} B_{on}^+ \left[\sum_{i=1}^I \cos \left(\frac{(n-1)\pi}{b_b} y_i \right) \cos \left(\frac{(m-1)\pi}{b_a} y_i \right) \Delta y_i \right]$$

$$- \sum_{i=1}^I H_i \cos \left(\frac{(m-1)\pi}{b_b} y_i \right) \Delta y_i = 0 \quad (z=L)$$

(N_m separate equations, m = 1, 2, . . . N_m) (50)

In contrast to equation (48), equation (50) has only the B_n^+ values as unknown representing the positive going waves. No negative waves are assumed in the exit. In addition, the exit occurs at z equals L ; however, the B^+ coefficients have been redefined as follows

$$B_n^+ e^{-jk_{zn}z} = B_n^+ e^{-jk_{zn}L} e^{-jk_{zn}(z-L)} = B_{on}^+ e^{-jk_{zn}(z-L)} \quad (51)$$

or

$$B_n^+ = B_{on}^+ e^{+jk_{zn}L} \quad (52)$$

In this manner, the exponential terms do not appear in equation (50).

Gradient at Inlet and Exit

The last boundary condition required concerns the gradient of H_x at the inlet and outlet of the nonuniform finite element region. In the finite element analysis to be developed in the next section, a contour integral term will be developed which will contain the term $\nabla H_x \cdot \bar{n}$. At a perfect conducting wall, it was shown that this term is identical to zero. However, along the entrance and exit interfaces, this term can be related to the modal equation in the analytical region. At the inlet

$$\nabla \tilde{H}_x \cdot \bar{n} = \left(\frac{\partial \tilde{H}_x}{\partial y} e_y + \frac{\partial \tilde{H}_x}{\partial z} e_z \right) \cdot (-e_z) = - \frac{\partial \tilde{H}_x}{\partial z} \quad (53)$$

while at the exit

$$\nabla \tilde{H}_x \cdot \bar{n} = + \frac{\partial \tilde{H}_x}{\partial z} \quad (54)$$

At the inlet and exit planes, continuity of the tangential component of the electric field is required across the interface (ref. 12, eq. 1.60). Employing equation (11) to express the tangential electric field in terms of the magnetic field (ref. 13, eq. 7-4) yields

$$\frac{\partial \tilde{H}_x}{\partial z} = \frac{\epsilon_T}{\epsilon_a} = \frac{\partial H_{xa}}{\partial z} \quad (55)$$

For the special cases where the properties remain constant across the interface, equations (53) and (54) simplify to the following forms:

$$\nabla \tilde{H}_x \cdot \bar{n} = - \frac{\partial H_{xa}}{\partial z} \quad (\text{inlet}) \quad (56)$$

and

$$\nabla \tilde{H}_x \cdot n = + \frac{\partial H_{xb}}{\partial z} \quad (\text{exit}) \quad (57)$$

In general, the gradient of the magnetic field is continuous except when there is a change in permittivity.

FINITE ELEMENT THEORY

The finite element formulation of the electromagnetic wave equation is now generated by using the Galerkin method (ref. 14) to obtain an integral form of the variable property wave equation over the whole (global) domain D shown in figure 5.

System Discretization

The continuous domain D is first divided into a number of discrete areas staked out by the nodal points as shown in figure 6. Although the nodal points are shown evenly spaced in figure 6, the advantage of finite element theory is that it allows the placement of nodes at any position desired. Another attractive feature of the finite element theory is the ability to change element properties in an easy manner.

Next, the continuous magnetic field component $H_x(y,z)$ will be approximated (curve fitted) in terms of the nodal potential values H_{xi} located at y_i, z_i , as shown in figure 6. The subscript i refers to any nodal point in this domain. The curve fit is required since the variable property wave equation will be integrated over the domain D shown in figure 5 and the curve fit will allow us to determine the value of H_x inside the element. This contrasts with the simplest form of finite difference theory (Taylor series) which usually only determines the values of the dependent variable at the lumped nodal points.

GLOBAL WEIGHTED RESIDUAL APPROACH

In the classical weighted residual manner, the magnetic field intensity component $H_x(y,z)$ is curve fitted by expanding in terms of all the unknown nodal values $H_{xi}(y_i, z_i)$ and a series of basis (shape) functions, such that

$$\tilde{H}_x(y,z) = \sum_{i=1}^N w_i(y,z) H_{xi} = [W] \{H_x\} \quad (58)$$

where the basis or weight functions $w_i(y,z)$ characterizes the spatial dependence of $\tilde{H}_x(y,z)$ in terms of H_{xi} which represents the unknown value of the magnetic field intensity component at the i nodal point in the global region. In the global approximation, the weight w_i has the property of being unity at node i and identical to zero at all other nodes. As before in equation (44) the hat over the $\tilde{H}_x(y,z)$ indicates that it is the approximate numerical solution to $H_x(y,z)$. The nodes are numbered $1, 2, \dots, N$ and the global vector $\{H_x\}$ represents the scalar values of the unknown magnetic intensity component H_x at each node, such that in matrix form

$$\{H_x\} = \begin{Bmatrix} H_{x1} \\ H_{x2} \\ \vdots \\ H_{x1} \\ \vdots \\ H_{xn} \end{Bmatrix} \quad \text{or} \quad \{H_x\}^T = [H_{x1} \ H_{x2} \ \dots \ H_{x1} \ \dots \ H_{xN}] \quad (59)$$

Since $\tilde{H}_x(y,z)$ is only an approximation to the true solution $H_x(y,z)$, substitution of equation (58) into the governing wave equation (26) and integrating over the domain D shown in figure 5 will not be equal to zero, as required by the exact solution but leave a residual error which is defined as R

$$\iint_D \left[\nabla \cdot \frac{1}{\epsilon_T} \nabla \tilde{H}_x + \omega^2 \mu \tilde{H}_x \right] dydz = R \quad (60)$$

In accordance with the method of weighted residuals, the assumed basis function W_i and the distribution of errors R are forced to be orthogonal ($R_i = 0$) within the region by letting

$$\iint_D W_i \left(\nabla \cdot \frac{1}{\epsilon_T} \nabla \tilde{H}_x + \omega^2 \mu \tilde{H}_x \right) dydz = 0$$

($i = 1, 2, \dots, N$ equations) (61)

Thus, there are n separate equations (written in compact form); one equation for each of the N nodal H_{xi} unknowns. In a direct analogy to the finite difference weighted residual control-volume formulation (ref. 15, p. 30), each of the above N equations represents a higher order difference approximation at the nodal point i where W_i has a value of unity.

By making use of the vector identity of a scalar ψ and a vector V

$$\nabla \cdot (\psi V) = \psi \nabla \cdot V + V \cdot \nabla \psi \quad (62)$$

and by letting ψ equal weight W_i and \bar{V} equal to $1/\epsilon_T \nabla \tilde{H}_x$, equation (61) can be expanded to

$$\iint_D \left[\nabla \cdot W_i \frac{1}{\epsilon_T} \tilde{H}_x - \frac{1}{\epsilon_T} \nabla \tilde{H}_x \cdot \nabla W_i + W_i \omega^2 \mu \tilde{H}_x \right] dydz = 0$$

($i = 1, 2, \dots, N$ equation) (63)

Finally, using the divergence theorem of Gauss (ref. 16, p. 79, eq. 4.7(b)),

$$\iint_D (\nabla \cdot V) \, dydz = \oint_S (V \cdot \bar{n}) \, ds \quad (64)$$

where \bar{n} is the unit outward normal vector to the boundary curve s , the first term in equation (63) can be converted into a surface integral such that

$$\iint_D \left[\frac{1}{\epsilon_T} \nabla W_i \cdot \nabla \tilde{H}_x - W_i \omega^2 \mu \tilde{H}_x \right] \, dydz - \oint_S \left(W_i \frac{1}{\epsilon_T} \nabla \tilde{H}_x \cdot \bar{n} \right) \, ds = 0$$

(i = 1, 2, . . . N equations) (65)

In effect, the second order differential equation has been reduced to a first order equation allowing the use of the weak formulation of the finite element theory. Thus in the Galerkin finite element approximation to follow, simple class C_0 shape functions can be employed to approximate W_i . Across an element shown in figure 6 for example, the class C_0 functions are only continuous in the dependent variable H_x and are discontinuous in slope. If the second order wave equation (61) is treated directly, then Hermitian calls C_1 functions are required to approximate W_i (ref. 7). In these class C_1 functions, both the variable and its slope are continuous across a boundary.

FINITE ELEMENT APPROXIMATION

Both the specification of the global weighting function W_i and the global integration over the whole domain D in figure 5 required by equation (65) are not practical. However, the integration can readily be performed by subdividing the domain into smaller elements A_e , defining the global shape function W_i in terms of the nodes of an individual element, integrating over an individual element and summing all the elements together.

Equation (65) is valid over the entire domain D shown in figure 5 or any subdomain A_e , as represented by the area of a small triangular element embedded in the region as depicted in figure 5. To begin the finite element aspect of the weighted residual method, the domain D is assumed to be divided into M elements defined by N nodes, see figure 6. In this case, equation (65) can be written as

$$\sum_{e=1}^M \iint_{A_e} \left(\frac{1}{\epsilon_{Te}} \nabla W_i \cdot \nabla \tilde{H}_x - \omega^2 \mu_e \tilde{H}_x W_i \right) \, dydz - \oint_S \left(W_i \frac{1}{\epsilon_{Te}} \nabla \tilde{H}_x \cdot \bar{n} \right) \, ds = 0$$

(i = 1, 2, . . . N equations) (66)

Where the properties are now given a subscript e to indicate that they may vary from element to element. Note, although the area integration in equation (66) applies to an individual element, the line integral is still defined over the global surface area, and as such, can be treated independently from the local area integrations.

LOCAL SHAPE FACTORS

Each element is defined by the nodes around its perimeter, while H_{xi} are defined at these nodes. However, the value of H_{xi} inside the element are required to perform the integration. To represent the variation inside the elements of the field variable H_x and its derivatives, local interpolation shape functions $N_j(y,z)$ for linear triangles are written in both scalar and matrix form as

$$\begin{aligned} \tilde{H}_x(y,z) &\equiv \tilde{H}_x^{(e)}(y,z) = N_1^{(e)}(y,z)H_{x1}^{(e)} + N_2^{(e)}(y,z)H_{x2}^{(e)} + N_3^{(e)}(y,z)H_{x3}^{(e)} \\ &= \sum_{j=1}^3 N_j^{(e)} H_{xj}^{(e)} = [N]^{(e)} \{H_x\}^{(e)} \end{aligned} \quad (67)$$

where $\{H_x\}^{(e)}$ is the vector of nodal values of H_x for a general element e with subscripts 1, 2, and 3 representing the nodal positions as shown in figure 5. The subscripts 1, 2, and 3 take on the actual nodal number of figure 6 when applied to a specific element.

The form of the local shape matrix $[N]^{(e)}$ depends on the type of element used. For the linear triangular element employed herein, the known value of $N_j^{(e)}$ is simple in form and can really be found in nearly every text on finite finite elements (ref. 6). Like its global counterpart W_j , the local $N_j^{(e)}$ has the property of being unity at node j and zero at the other nodes in the triangle. A graphical description of N is shown in figure 3 of reference 14. Replacing \tilde{H}_x by $\tilde{H}_x^{(e)}$ in equation (66), the new governing finite element equations became

$$\begin{aligned} \sum_{e=1}^M \iint_{Ae} \left(\frac{1}{\epsilon_{Te}} \nabla W_1 \cdot \nabla \tilde{H}_x^{(e)} - W_1 \omega^2 \mu_e \tilde{H}_x^{(e)} \right) dydz - \oint_S \left(W_1 \frac{1}{\epsilon_{Te}} \nabla \tilde{H}_x^{(e)} \cdot \bar{n} \right) ds = 0 \\ (i = 1, 2, \dots, N \text{ equations}) \end{aligned} \quad (68)$$

GALERKIN APPROXIMATION

The weight $W_1(y,z)$ is now approximated by multiple values of $N_j^{(e)}$ (see ref. 14, fig. 3). Adapting the Galerkin approximation to the more general weighted residual approach assumes that

$$W_1(y,z) = N_1^{(e)}(y,z) \quad (69)$$

in all elements containing the 1 node. For all elements which do not contain the node 1, the weight W_1 is assumed zero not only at all other nodes (as required by the general definition of W_1) but also at all values of y and z in the elements which do not contain the node 1.

Recognizing that $N_1^{(e)}$ is zero for all elements not having the unknown H_{x1} associated with a particular element, the finite element equation (68) can now be written in compact form as

$$\sum_{e=1}^M \iint_{Ae} \left(\frac{1}{\epsilon_{Te}} \nabla N_1^{(e)} \cdot \tilde{\nabla} H_x - N_1^{(e)} \omega^2 \mu_e \tilde{H}_x^{(e)} \right) dydz - \oint_C \left(N_1^{(e)} \frac{1}{\epsilon_{Te}} \tilde{\nabla} H_x^{(e)} \cdot \bar{n} \right) ds = 0$$

(1 = 1, 2, . . . N equations) (70)

where N_1 are the known shape functions (ref. 6, eq. (3.05)). In general most of the M elements in the summation will have zero contribution, since only if the i mode is part of the element will $N_1^{(e)}$ have a nonzero value. Likewise, the line integral can only contribute to a particular i equation, if the node is on the boundary. For all interior nodes, the line integral term in equation (70) will not contribute, since $N_1^{(e)}$ will have a zero value on the boundary.

SURFACE INTEGRAL AND BOUNDARY CONDITIONS

The surface integral in equation (70) can be rewritten along the boundary in figure 5 as

$$\oint_S \left(N_1^{(e)} \frac{1}{\epsilon_{Te}} \tilde{\nabla} H_x^{(e)} \cdot \bar{n} \right) ds = \int_{\text{Entrance}} N_1^{(e)} \frac{1}{\epsilon_{Te}} \left(\tilde{\nabla} H_x \cdot \bar{n} \right) ds$$

$$+ \int_{\text{Exit}} N_1^{(e)} \frac{1}{\epsilon_{Te}} \left(\tilde{\nabla} H_x \cdot \bar{n} \right) ds + \int_{\text{PEC}} N_1^{(e)} \frac{1}{\epsilon_{Te}} \left(\tilde{\nabla} H_x \cdot \bar{n} \right) ds \quad (71)$$

As shown in equation (42), the gradient dotted into the outward normal is identical to zero along a perfect electrical conductor (PEC); thus, the last surface integral on the right hand side of equation (71) is identical to zero. In addition, at the entrance, the axial derivatives in the line integral at the entrance and exit planes represent the value of slope just inside the finite element domain. They can be related to the slopes in the analytical region through boundary condition equations (56) and (57). Therefore,

$$\oint \left(N_1^{(e)} \frac{1}{\epsilon_{Te}} \tilde{\nabla} H_x^{(e)} \cdot \bar{n} \right) ds = - \int_{\text{Entrance}} N_1^{(e)} \frac{1}{\epsilon_{Te}} \left. \frac{\partial \tilde{H}_x}{\partial z} \right|_{z=0} dy$$

$$+ \int_{\text{EXIT}} N_1^{(e)} \frac{1}{\epsilon_{Te}} \left. \frac{\partial \tilde{H}_x}{\partial z} \right|_{z=L} dy = 0 \quad (72)$$

Thus, the finite element equation (70) can be rewritten as

$$\sum_{e=1}^M \iint_{Ae} \left(\frac{1}{\epsilon_{Te}} \nabla N_1^{(e)} \cdot \tilde{\nabla} H_x^{(e)} - N_1^{(e)} \omega^2 \mu_e H_x^{(e)} \right) dydz + \int_{\text{Entrance}} N_1^{(e)} \frac{1}{\epsilon_{Te}} \left. \frac{\partial \tilde{H}_x}{\partial z} \right|_{z=0} dy$$

$$- \int_{\text{Exit}} N_1^{(e)} \frac{1}{\epsilon_{Te}} \left. \frac{\partial \tilde{H}_x}{\partial z} \right|_{z=L} dy = 0 \quad (73)$$

(1 = 1, 2, . . . N equations)

where the gradients in the finite element region in equation (73) at the entrance and exit planes can be related to gradients in the entrance and exit ducts, equations (32) and (34) through equation (55).

FINITE ELEMENT EQUATIONS

Expanding $\tilde{H}_x^{(e)}$ in terms of the weighting function equation (67), and neglecting the surface integrals for simplicity in writing (exact for central elements), equation (73) becomes

$$\sum_{e=1}^M \{H_x\}^{(e)} \iint_{A_e} \left\{ \frac{1}{\epsilon_{Te}} N_i^{(e)} \cdot [\nabla N]^{(e)} - \omega^2 \mu_e N_i^{(e)} [N]^{(e)} \right\} dydz = 0$$

(i = 1, 2, . . . N equations) (74)

where the $\{H_x\}^{(e)}$ local magnetic field intensity component column vector can be pulled outside the area integration since it does not depend on the area coordinates.

Equation (74) could in principle be evaluated for each i to yield a set of N simultaneous equations for the N unknown value of H_{xi} . However, this approach is not readily implemented on a digital computer. Rather, each element is treated independently and the contributions of a single element to all N equations defined by equation (74) are determine simultaneously from the following

$$\{H_x\}^{(e)} \iint_{A_e} \left\{ \frac{1}{\epsilon_{Te}} \nabla N_j^{(e)} \cdot [\nabla N]^{(e)} - \omega^2 \mu_e N_j^{(e)} [N]^{(e)} \right\} dydz = 0$$

(j = 1, 2, 3) (75)

In contrast to the i subscript of equation (74) for all nodes in the global domain, here the subscript j sums only the three nodes of a particular element. In compact standard finite element form, equation (75) can be rewritten as

$$[K]^{(e)} \{H_x\}^{(e)} = 0$$

(76)

where

$$K_{ij}^{(e)} = \frac{1}{\epsilon_{Te}} \iint_{A_e} \left[N_{iy}^{(e)} N_{jy}^{(e)} + N_{iz}^{(e)} N_{jz}^{(e)} - k_e^2 N_i^{(e)} N_j^{(e)} \right] dydz = 0$$

(77)

with

$$k_e^2 = \omega^2 \mu_e \epsilon_{Te}$$

(78)

For triangular elements, the evaluation of equation (77) is quite simple and presented in many texts (ref. 18, p. 149, eq. (8.42) for the first two terms and page 45 for the last term). The surface integral is evaluated in a similar manner. Shortly, a discussion is given on how equation (76) is used to build up equation (74).

MODAL COEFFICIENTS

In addition to the N finite element global equations (eq. 74) required to determine \tilde{H}_{x1} values, additional equations are required for each unknown value $A_{\bar{n}}$ and $B_{\bar{n}}^+$ which describe H_x in the analytical entrance and exit region to the finite element domain. The unknown coefficient $A_{\bar{n}}$ and $B_{\bar{n}}^+$ couple to the finite element domain through the surface integral terms in equation (73). For convenience in the finite element solution, the unknown nodal coefficients $A_{\bar{n}}$ and $B_{\bar{n}}^+$ are incorporated into the global unknown vector $\{\Phi\}$ such that

$$\{\Phi\}^T = \left[A_1^- \ A_2^- \ \dots \ A_{N_m}^- \ \tilde{H}_{x1}, \ \tilde{H}_{x2}, \ \dots \ \tilde{H}_{x1} \ \dots \ \tilde{H}_{xN} \ B_1^+ B_2^+ \ \dots \ B_{N_m}^+ \right] \quad (79)$$

GLOBAL FINITE ELEMENT EQUATIONS

Along with equations (48) and (50) which define the modes in the analytical region, using the standard finite element procedures (ref. 18) the elemental equation (76) can be assembled into equation (74) to yield the following global set of simultaneous equations which can be solved to obtain the unknown modal intensities \tilde{H}_{x1} and unknown coefficient $A_{\bar{n}}$ and $B_{\bar{n}}^+$:

$$[K] \{\Phi\} = \{F\} \quad (80)$$

Here, the column vector F contains boundary condition information which includes input modal condition A^+ (right hand side of equation (48)). The global stiffness matrix $[K]$ is the sum of the known local stiffness matrix $[K](e)$ defined by equation (77). The solution of equation (80) by a banded Gauss solver yields Φ .

Next, the solution of equation (80) for a number of element discretization patterns, absorber materials and nodal inputs will be considered.

RESULTS AND COMPARISONS

For theory and code validation, first the finite element solutions will be applied to a number of problems where exact solutions exist. Next, the finite element solutions will be applied to a number of problem with various types of absorbers mounted on the walls.

In all the examples to follow, the properties of the entrance region are assumed to be unity

$$\begin{aligned} \epsilon_1 &= 1 \\ \mu_1 &= 1 \end{aligned} \quad (81)$$

In addition, the length of the finite element domain and height of the entrance duct are held at unity.

For the linear element considered herein, the minimum required elements in the axial and transverse direction can be calculated from a formula developed to give reasonable accuracy (ref. 7, eq. 48) using finite difference theory.

$$\text{Number axial element} \geq 12 L \omega / 2\pi \quad (82)$$

$$\text{Number transverse elements} \approx 12 (n - 1) \quad n \geq 2 \quad (83)$$

where n is the highest transverse mode to be resolved. In each example, a pictorial of the grid discretization is shown directly above the plots of the H_x spatial variations.

Example 1. - Plane Wave Propagation in Perfectly Conducting Duct

As the first example of the finite element technique, consider the problem of an infinite long duct with perfectly conducting walls and with a plane H_x wave propagating to the right from $-$ infinity with a frequency of $\omega = 2\pi$. For this case, the wave continues propagating to $+$ infinity without producing any reflected waves. The exact analytical expression for H_x can be written (ref. 11, p. 457) as

$$|H_x| = e^{-jk_1 x} = \cos 2\pi x - i \sin 2\pi x \quad (84)$$

As seen in figure 7, a comparison between the exact analytical results and the finite element analysis shows very good agreement between both analysis. The finite element analysis predicted A^- coefficients of zero for the entrance region (no reflections) and unity for the B_1^+ coefficient while higher order B^+ coefficients were appropriately near zero.

Figure 8 applies to the same example only the magnitude of the H_x wave is displayed where the magnitude H_x is defined as

$$|H_x| = \sqrt{\text{Re}(H_x)^2 + \text{Im}(H_x)^2} \quad (85)$$

Figure 9 displayed the axial flux of energy (Poynting vector) defined by (ref. 11, eq. (8-69))

$$P_{\text{ave}}(y, z) = \frac{1}{2} \text{Re} (E \times H^*) \quad (86)$$

$$P_{\text{ave}}(y, z) = \frac{1}{2} \text{Re} \frac{1}{\omega \epsilon_T} H_x^* \frac{\partial H_x}{\partial z} \quad (87)$$

The total power radiated down the duct is given by

$$P_T = \int_S P_{\text{ave}}(y, z) dy \quad (88)$$

In all cases, the inlet total power is normalized as unity. Thus as expected in figure 9, the total power remains at a unity value throughout the duct.

According to equation (87), the gradient of H_x is required to determine the Poyning vector. In the analytical entrance and exit regions the gradient can, of course, be determined exactly from the known analytical expressions. However, in the finite element region some error is introduced since the gradient is a constant throughout a triangular element (ref. 18, p. 30). This requires many small elements to approximate a rapid change in the variable H_x . However, if only the transmitted and reflected energy are required a coarse finite element grid will suffice, since the analytical expressions for the derivatives are known exactly. In figure 9, the small error in the finite element region ($z = 0$ to 1) results from the coarse elements, smaller elements will reduce this error.

Example 2. - Third Propagating Mode in Perfectly Conducting Duct

As the second example of the finite element technique, again consider the problem of an infinitely long duct with perfectly conducting walls and the TM_{30} (A_3^+) wave propagating to the right from $-$ infinity with a frequency of $\omega = 6.911$ ($f = 1.1$). Again for this case the wave continues propagating to $+$ infinity without producing any reflected waves. The exact analytical expression for TM_{30} can be written according to equations (30) and (29) as

$$k_{z3} = 2\pi \times 1.1 \sqrt{1 - \left(\frac{(3-1)(\pi)}{2\pi \times 1.1} \right)^2} = 2.881 \quad (89)$$

$$H_x = e^{-jk_{z3}z} = \cos 2.881z - j \sin 2.881z \quad (y = 0) \quad (90)$$

where the frequency of the wave has been increased over the value of 1 in example 1 to 1.1 so that the third mode is now propagating while the fourth mode is cut off.

Again, as seen in figure 10 for the real and imaginary parts of H_x , and in figure 11 for the magnitude of H_x , the finite element and exact analytical results are in good agreement.

Example 3. - Reflection, Transmission, and Absorption of Plane Waves

As our next set of validation problems, consider the phenomenon of reflection which occurs when a uniform plane wave is normally incident on the boundary between regions composed of two different materials, as shown in figure 12. The exact analytical results are given in standard textbooks. However, the exact analytical results have been slightly modified to account for the fact that the incident plane wave contacts the interface at z equal to L_d .

The exact analytical equations can be written in the following form

$$H_x^{(1)} = H_{x1} + H_{xr} \quad (z < L_d) \quad (91)$$

$$H_{x1} = H_{i0} e^{-\gamma_1 z} \quad (z < L_d) \quad (92)$$

$$H_{xr} = H_{r0} e^{+\gamma_1 z} \quad (z < L_d) \quad (93)$$

$$H_x^{(2)} = H_{xt} = H_{t0} e^{-\gamma_2 z} \quad (z > L_d) \quad (94)$$

where the magnetic field in region (1) $H_x^{(1)}$ is composed of an incident field H_{x1} and a reflected field H_{xr} whose magnitudes and propagation constants are defined in equations (92) and (93) with

$$\gamma_1 = +j\omega\sqrt{\mu_1\epsilon_1} \quad (\epsilon_{c1} = 0) \quad (95)$$

In region (2), $H_x^{(2)}$ is composed only of a transmitted magnetic intensity deferred by equation (94) with

$$\gamma_2 = \alpha_2 + j\beta_2 = +j\omega\sqrt{\mu_2\epsilon_2} \sqrt{1 - j\frac{\epsilon_{c2}}{\epsilon_2}} \quad (96)$$

(ref. 19, p. 388, eq. (32)). For convenience in obtaining numerical results, γ_2 has been expressed in terms of α_2 (real part) and β_2 (imaginary part). Or solving for α_2 and β_2 (ref. 11, p. 364 P. 8-6 or ref. 12, p. 2-1)

$$\beta_2 = \omega\sqrt{\frac{\mu_2\epsilon_2}{2}} \left[1.0 + \sqrt{1 + \left(\frac{\epsilon_{c2}}{\epsilon_2}\right)^2} \right]^{1/2} \quad (97)$$

$$\alpha_2 = \frac{\omega^2\epsilon_{c2}\mu_2}{2\beta_2} = \omega\sqrt{\frac{\mu_2\epsilon_2}{2}} \left[\sqrt{1 + \left(\frac{\epsilon_{c2}}{\epsilon_2}\right)^2} - 1 \right]^{1/2} \quad (98)$$

At $z = L_d$, the magnetic intensity in region (1) must be equal to the magnetic intensity in region (2); consequently, equations (91) and (92) are equated. Likewise, the incident and reflected electric fields in region (1) must be equal to the transmitted electric field in region (2). The electric fields can be expressed in terms of the magnetic fields by employing Maxwell's equations. These two conservation equations can now be solved for the unknown reflected H_{r0} and transmitted H_{t0} wave magnitudes in terms of the known incident magnitude H_{i0}

$$\frac{H_{r0}}{H_{i0}} = \Gamma e^{-2\gamma_1 L_d} \quad (99)$$

$$\frac{H_{t0}}{H_{i0}} = \tau e^{-(\gamma_1 - \gamma_2)L_d} \quad (100)$$

with the reflection Γ and transmission τ coefficient defined as

$$\Gamma = \frac{\eta_1 - \eta_2}{\eta_2 + \eta_1} \quad (101)$$

(ref. 13, eq. 5-97)

$$\tau = \frac{2\eta_1}{\eta_2 + \eta_1} \quad (102)$$

(ref. 13, eq. 5-98)

The impedance η_1 and η_2 have the usual convenient definitions (for positive values)

$$\eta = - \frac{E_y}{H_x} \quad (103)$$

(ref. 13, eq. 7-50)

$$\eta_1 = - \frac{\frac{1}{j\omega\epsilon_{T1}} \nabla \times H}{H_x} = - \frac{\frac{1}{j\omega\epsilon_{T1}} \frac{\partial H_x}{\partial z}}{H_x} = \sqrt{\frac{\mu_1}{\epsilon_1}} \quad (104)$$

$$\eta_2 = \frac{+ \frac{E_y}{1}}{j\omega\mu_2} = - \frac{j\omega\mu_2 E_y}{\frac{\partial E_y}{\partial z}} = \frac{+j\omega\mu_2}{\gamma_2} \quad (105)$$

The first case will consider a step change in permittivity from 1 to 4 at z equal to 0.25. As shown in figure 13, the z equals 0.25 interface occurs in the third row of elements which have been decreased in size to account for the smaller wave length in the higher permittivity material. As seen in figure 13, the finite element and exact analytical theories are in excellent agreement. Note the shift in slope of the real component at the interface which is automatically accounted for in the theory, because of variable property assumption in equation (26). Figure 14 shows similar good agreement between the finite element theory and the exact analytical results for the absolute magnitude of the magnetic intensity H_x . The reflections from the interface are clearly represented by the standing wave pattern ahead of the interface. Observe that the magnitude of H_x increases in the material. The opposite effect will be seen in the next example.

The second case considers a step change in permeability from 1 to 4 at z equals to 0.05. In this case, the interface occurs immediately after the very first row of elements shown in figure 15. As seen in figure 15, the finite element and exact analytical theories are in excellent agreement. For this particular example the slope is continuous throughout both domains as expected since equation (55) indicates that the slope is continuous for changes in permeability. Figure 16 shows similar good agreement between the

finite element theory and the exact analytical results for the absolute magnitude of the magnetic intensity H_x . Again the reflections are clearly represented by the standing wave pattern ahead of the interface. In contrast to be previous example, the magnitude of H_x decrease in the material.

The final case considers a step change in conductivity from 0 to 2 at z equals 0.0. The jump in properties at $z = 0$ is handled through equation (55) which is employed in the entrance and exit integrals of equation (73). As seen in figure 17 a slight difference in the magnitude between the finite element and analytical results occurs. The analytical solution was developed from a three region model (ref. 11, p. 347). A similar curve was obtained when the step change in conductivity was placed at $z = 0.25$ inside the finite element region. Figure 18 shows a similar discrepancy for the Poynting vector. The error could not be eliminated with finer grid; therefore, it was assumed that the errors are a result of the discretization process which must be resolved.

Example 4. - Wall Absorbers

Figure 19 shows a configuration with an absorber region along the upper wall. For a wall material with a permeability of 1 and total permittivity of $1.-j2.$, the energy attenuation is shown in figure 20. In figure 21, wall absorbers are placed at the top and bottom of the duct. For wall material with a permeability of 4.1 and permittivity of $1.-j 2.83$, the wall absorption is shown in figure 22.

Figure 23 displays contour plots of the magnitude of the magnetic field for the absorber configuration shown in figure 21. The solid line drawing show the complete contours, while the symbol are plotted at selective points in the companion figure so that the actual magnitude of the contour can be readily determined. For convenience the magnitude of the magnetic field has been renormalized between 0 and 1 according to the formula

$$\left| H_{x \text{ contour}} \right| = \frac{|H_x| - |H_{x \text{ min}}|}{|H_{x \text{ max}}| - |H_{x \text{ min}}|} \quad (106)$$

where $H_{x \text{ max}}$ is the maximum value of magnitude of the magnetic field in the plotting domain and $H_{x \text{ min}}$ is the minimum value of H_x in the plotting domain.

In figure 23(a) only one mode (plane wave) is assumed in the modal expansion. In this case,

$$\left| A_1^+ \right| = 1.0 \quad \left| A_1^- \right| = 0.231 \quad \left| B_1^+ \right| = 0.458$$

and the value of the Poynting vector at the exit has fallen from 1 to 0.210. In figure 23(b) three modes are assumed in the modal expansion. In this case,

$$\begin{aligned} \left| A_1^+ \right| &= 1.0 & \left| A_1^- \right| &= 0.1426 & \left| B_1^+ \right| &= 0.598 \\ \left| A_2^+ \right| &= 0.0 & \left| A_2^- \right| &= 0.475 \times 10^{-5} & \left| B_2^+ \right| &= 0.98 \times 10^{-5} \end{aligned}$$

$$|A_3^+| = 0.0 \quad |A_3^-| = 0.664 \quad |B_3^+| = 1.123$$

Because of the symmetrical nature of the magnetic field, the odd eigenfunctions have near zero coefficients. For this case, the Poynting vector at the exit has obtained a value of 0.358.

In the contour plot example shown in figure 23(c), five modes are assumed in the modal expansion. In this case,

$$\begin{aligned} |A_1^+| &= 1.0 & |A_1^-| &= 0.1246 & |B_1^+| &= 0.6501 \\ |A_2^+| &= 0.0 & |A_2^-| &= 0.186 \times 10^{-4} & |B_2^+| &= 0.571 \times 10^{-5} \\ |A_3^+| &= 0.0 & |A_3^-| &= 0.6457 & |B_3^+| &= 1.175 \\ |A_4^+| &= 0.0 & |A_4^-| &= 0.376 \times 10^{-5} & |B_4^+| &= 0.398 \times 10^{-5} \\ |A_5^+| &= 0.0 & |A_5^-| &= 0.0145 & |B_5^+| &= 0.0264 \end{aligned}$$

For this case the Poynting vector at the exit was 0.423.

As seen in figure 23(c), the magnetic field has decreased to near zero at the walls but remains relatively high in the center of the duct. In effect, electromagnetic energy beams through the center of the duct. Future work will consider reducing the energy of this central beam.

Finally, in the last contour plot example, seven modes are assumed in the modal expansion. This contour plot was for practical purposes identical to the plot shown in figure 23(c). In this case, the modal coefficients are

$$\begin{aligned} |A_1^+| &= 1.0 & |A_1^-| &= 0.1204 & |B_1^+| &= 0.659 \\ |A_2^+| &= 0.0 & |A_2^-| &= 0.078 \times 10^{-4} & |B_2^+| &= 1.185 \times 10^{-5} \\ |A_3^+| &= 0.0 & |A_3^-| &= 0.6416 & |B_3^+| &= 1.160 \\ |A_4^+| &= 0.0 & |A_4^-| &= 0.555 \times 10^{-5} & |B_4^+| &= 0.951 \times 10^{-5} \\ |A_5^+| &= 0.0 & |A_5^-| &= 0.0141 & |B_5^+| &= 0.0252 \\ |A_6^+| &= 0.0 & |A_6^-| &= 0.799 \times 10^{-6} & |B_6^+| &= 0.959 \times 10^{-6} \\ |A_7^+| &= 0.0 & |A_7^-| &= 0.00286 & |B_7^+| &= 0.00528 \end{aligned}$$

and the normalized Poynting vector at the exit was 0.435, which is very close to the value when five modes were assumed. In this seven mode expansion, the modal amplitudes of the first five modes are reasonably close to the values when a five mode expansion was assumed. In addition, the amplitude of the seventh mode is very small. Therefore, a five mode expansion leads to convergence.

Example 5. - Thin Layer Absorbers

The code has a zoom feature as shown in figure 24 for which the thin layered region is expanded for ease in visualization. Now, any desired properly variation in the material can be conveniently reproduced.

Figure 25 displays a multiple thin film region analyzed. The attenuation of the region is shown in figure 26.

CONCLUDING REMARKS

The finite element method has been developed to handle the problem of electromagnetic propagation in a duct with varying wall properties and geometries. The numerical formulation is relatively simple to use and appears to give very accurate results. For higher frequencies many wave lengths will exist in the duct requiring a large number of elements. With the expanded memory capability of the modern computer, the restriction does not represent a severe limitation of the method.

REFERENCES

1. Kennedy, G., Electronic Communication Systems, 3rd ed., McGraw-Hill, New York, 1985.
2. Lee, C.S., Chuang, S.L., and Lee, S.W., "A Simple Version of Corrugated Waveguide: Smooth-Walled Circular Waveguide Coated with Lossy Magnetic Material," AP-S International Symposium Digest, Vol. 1, IEEE, New York, 1985, pp. 303-306.
3. Taflove, A. and Brodwin, M.E., "Numerical Solution of Steady-State Electromagnetic Scattering Problems Using the Time-Dependent Maxwell's Equations," IEEE Transactions on Microwave Theory and Techniques, Vol. MTT-23, No. 8, Aug. 1975, pp. 623-630.
4. Taflove, A. and Umashankar, K., "A Hybrid Moment Method/Finite Difference Time Domain Approach to Electromagnetic Coupling and Aperture Penetration into Complex Geometries," IEEE Transactions on Antennas and Propagation, Vol. AP-30, No. 4, July 1982, pp. 617-627.
5. Rice, E.J., Attenuation of Electromagnetic Energy in Ducts-Approximate Equations and Optimum Wall Properties, to be published.
6. Silvester, P.P. and Ferrari, R.L., Finite Elements For Electrical Engineers, Cambridge University Press, Cambridge, England, 1983.
7. Baumeister, K.J., "Numerical Techniques in Linear Duct Acoustics - A Status Report," Journal of Engineering for Industry, Vol. 103, No. 3, Aug. 1981, pp. 270-281.
8. Baumeister, K.J., "Application of a Finite-Difference Technique to Thermal Wave Propagation," Heat Transfer-Research and Application, J.C. Chen, ed., AICHE Symposium Series, Vol. 74, No. 174, 1978, 243-249.

9. Baumeister, K.J., Eversman, W., Astley, R.J. and White, J.W., "Acoustics in Variable Area Duct: Finite Element and Finite Difference Comparison to Experiment," AIAA Journal, Vol. 21, No. 2, Feb. 1983, pp. 193-199.
10. Jakob, M., Heat Transfer, Vol. I, Wiley, New York, 1962.
11. Cheng, D. K., Field and Wave Electromagnetics, Addison-Wesley, Reading, 1983.
12. Kraichman, M.B., Handbook of Electromagnetic Propagation in Conducting Media, NAVMAT P-2302, U.S. Government Printing Office, Washington, D.C., 1970.
13. Jordan, E.C. and Balmain, K.G., Electromagnetic Waves and Radiating System, 2nd ed., Prentice-Hall, Englewood Cliffs, 1968.
14. Baumeister, K.J., "Effect of Triangular Element Orientation on Finite Element Solutions of the Helmholtz Equation," NASA TM-87351, 1980.
15. Patankar, S.V.; and Shih, T.M., Numerical Heat Transfer and Fluid Flow, McGraw-Hill, New York, 1980.
16. Martin, H.C. and Carey, G.F., Introduction to Finite Element Analysis, McGraw-Hill, New York, 1973.
17. Lester, H.C. And Parrott, T.L., "Application of a Finite Element Methodology for Computing Grazing Incidence Wave Structure in an Impedance Tube: Comparison with Experiment," AIAA Paper 79-0664, Mar. 1979.
18. Segerlind, L.J., Applied Finite Element Analysis, John Wiley and Sons, New York, 1976.
19. Hayt, W.H., Engineering Electromagnetics, McGraw-Hill, New York, 1981.

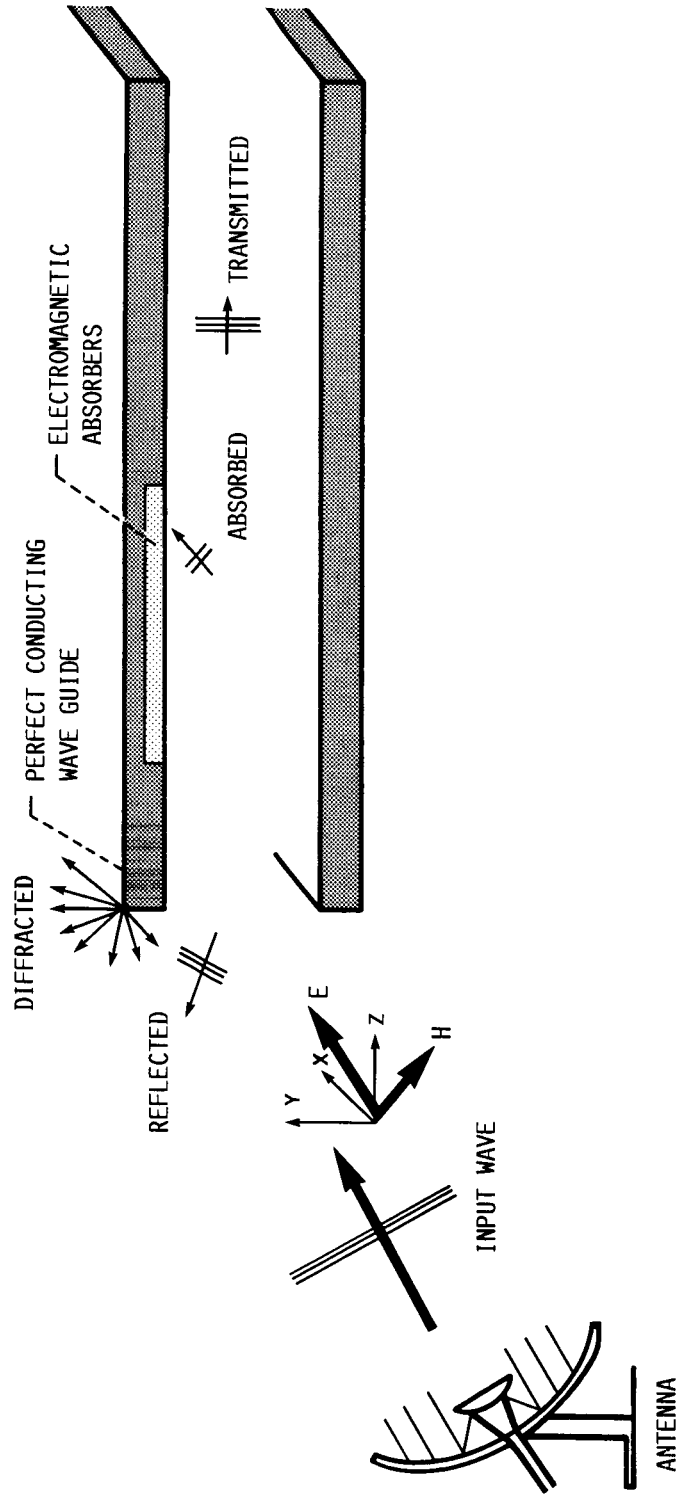


FIGURE 1.- SCHEMATIC OF ELECTROMAGNETIC PROPAGATION IN A TWO DIMENSIONAL ABSORBING WAVE GUIDE.

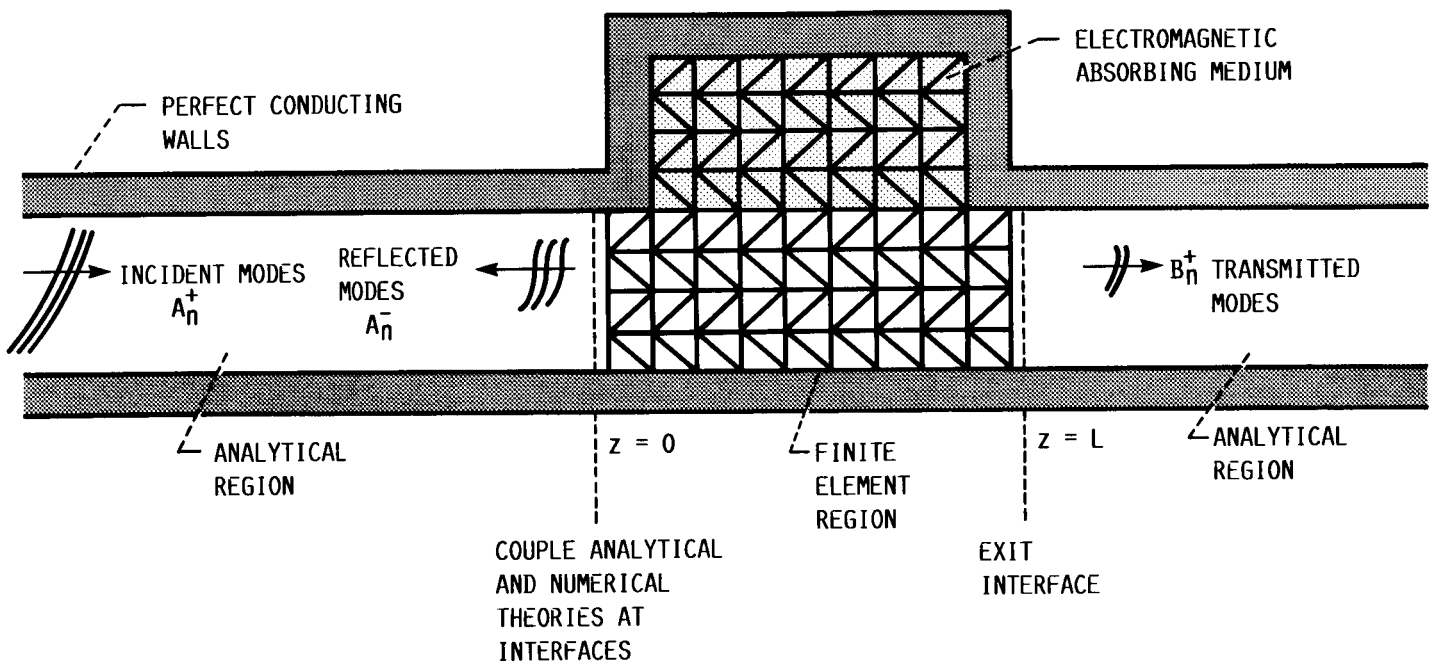


FIGURE 2.- TWO DIMENSIONAL WAVE GUIDE FINITE ELEMENT MODEL.

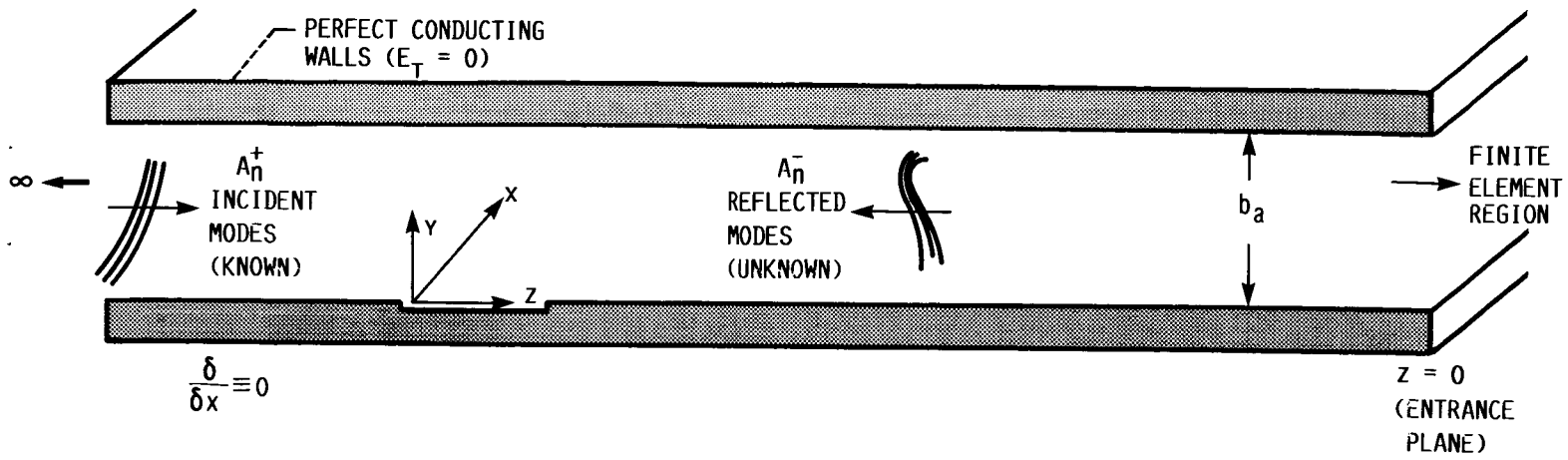


FIGURE 3.- ENTRANCE GEOMETRY FOR ANALYTICAL SOLUTION REGION.

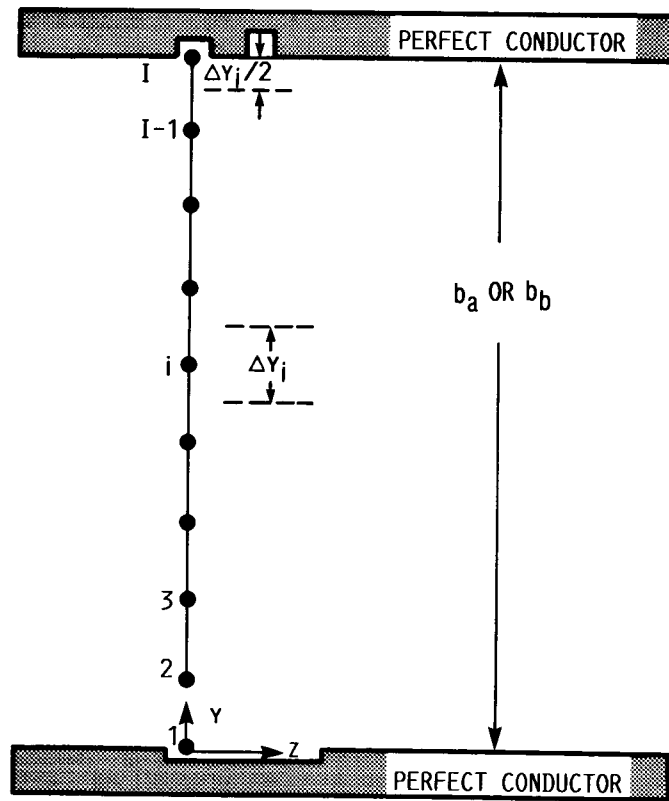


FIGURE 4.- AREA INTEGRATION FOR THE INTERFACE CONTINUITY EQUATION.

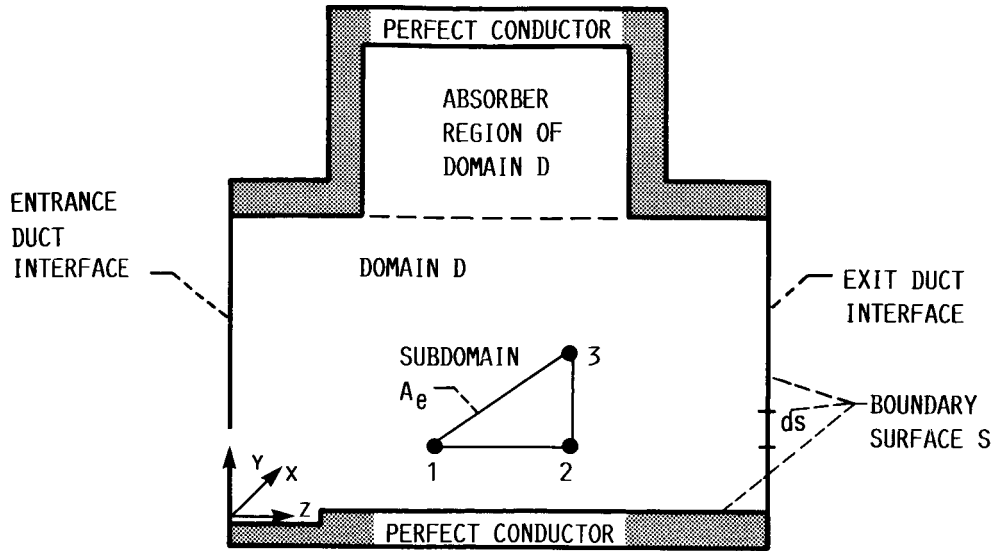


FIGURE 5.- ELECTROMAGNETIC BOUNDARY VALUE FORMULATION.

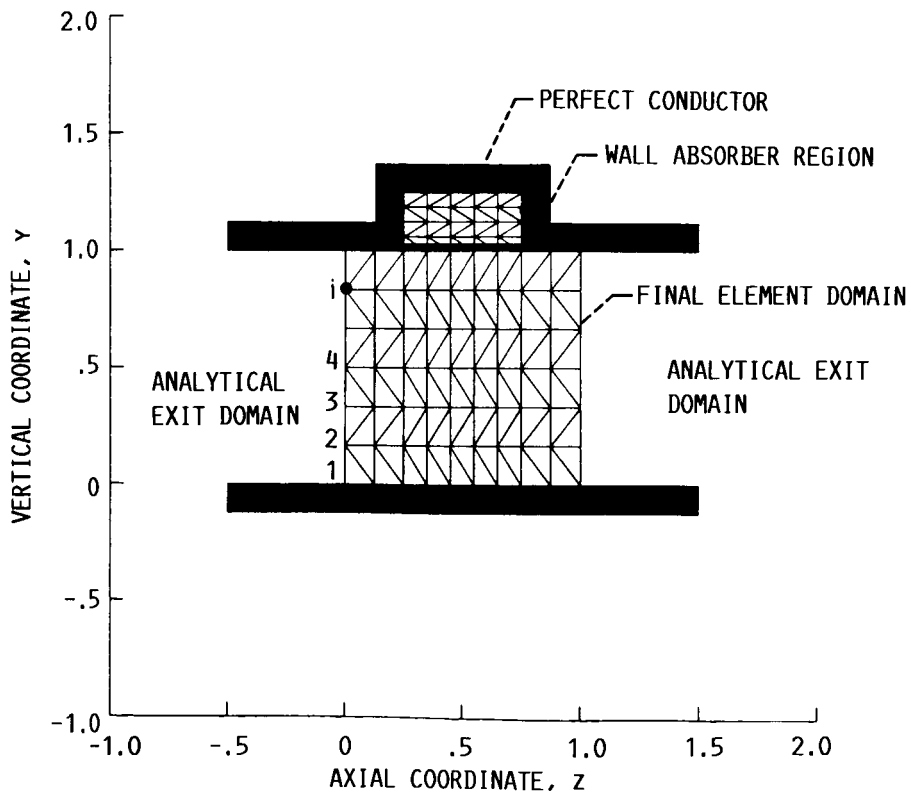


FIGURE 6.- DISCRETIZATION OF SOLUTION DOMAIN USING TRIANGULAR ELEMENTS.

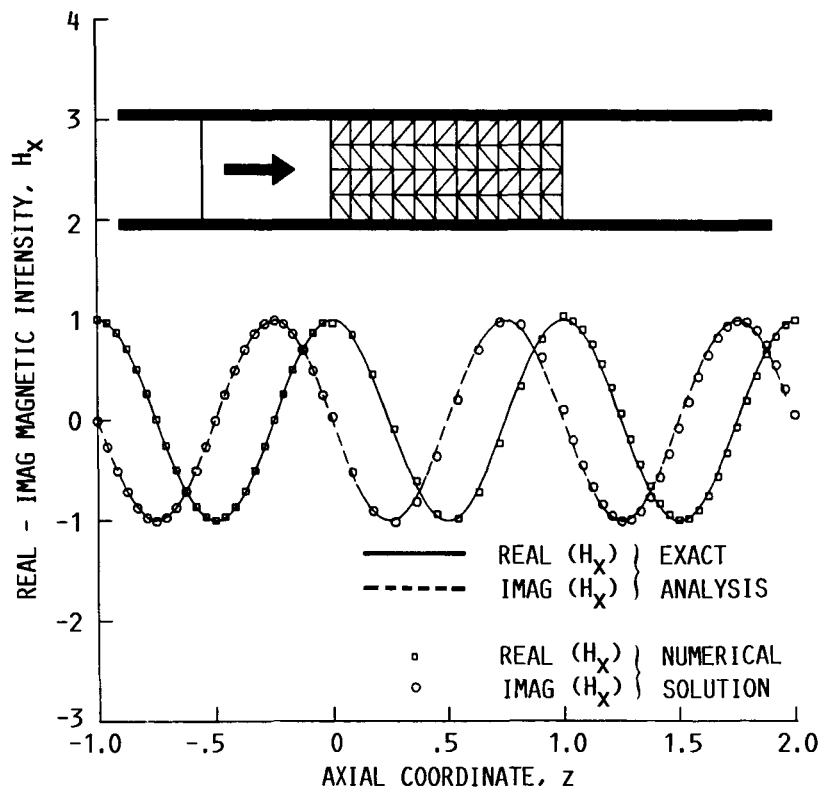


FIGURE 7. - A COMPARISON OF THE AXIAL MAGNETIC INTENSITY VARIATION ALONG THE LOWER WALL IN A UNIFORM DUCT WITH PERFECTLY CONDUCTING WALLS AS OBTAINED BY USING AN EXACT SOLUTION AND A FINITE ELEMENT SOLUTION FOR A PLANE WAVE (MODE 1) INCIDENT AT $z = 0$ WITH $\omega = 2\pi$.

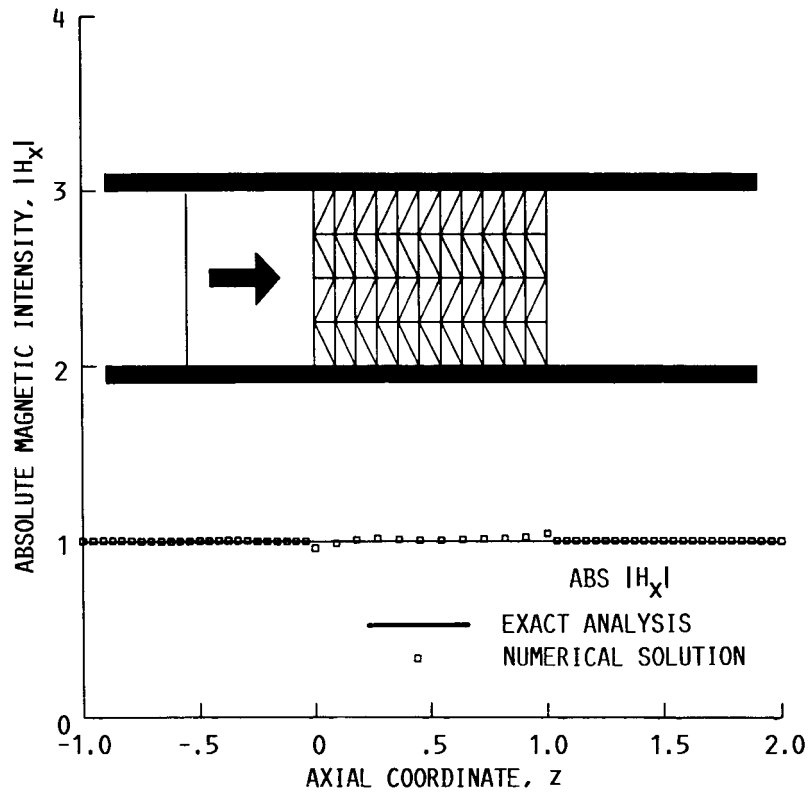


FIGURE 8.- A COMPARISON OF THE MAGNITUDE OF THE AXIAL MAGNETIC INTENSITY VARIATION ALONG THE LOWER WALL IN A UNIFORM DUCT WITH PERFECTLY CONDUCTING WALLS AS OBTAINED BY USING AN EXACT SOLUTION AND A FINITE ELEMENT SOLUTION FOR A PLANE WAVE (MODE 1) INCIDENT AT $z = 0$ WITH $\omega = 2\pi$.

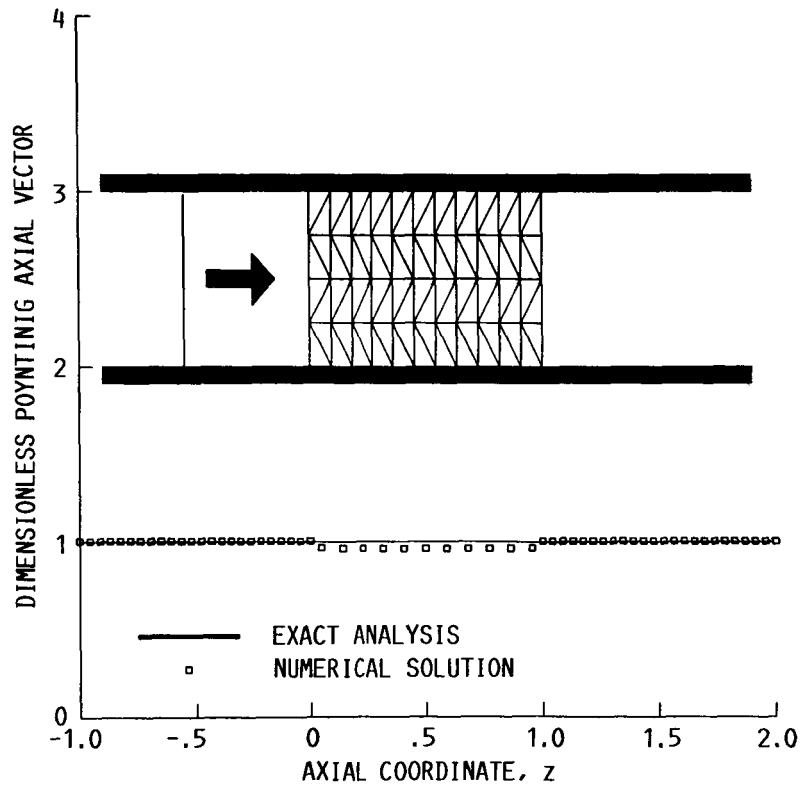


FIGURE 9. - A COMPARISON OF THE AXIAL FLUX OF ENERGY (POYNING VECTOR) VARIATION IN A UNIFORM DUCT WITH PERFECTLY CONDUCTING WALLS AS OBTAINED BY USING AN EXACT SOLUTION AND A FINITE ELEMENT SOLUTION FOR A PLANE WAVE (MODE 1) INCIDENT AT $z = 0$.

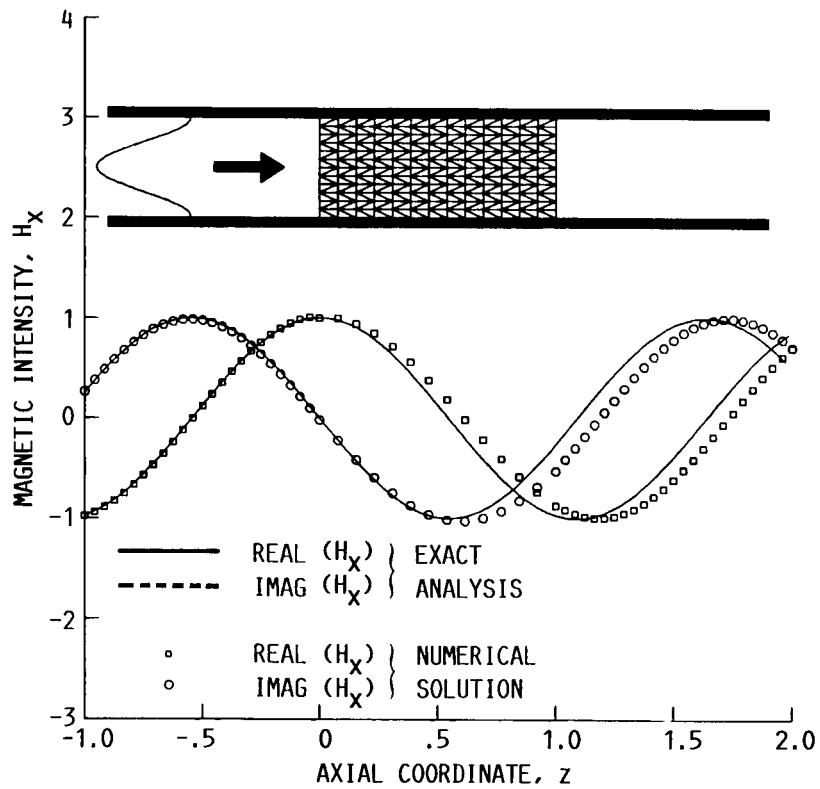


FIGURE 10. - A COMPARISON OF THE AXIAL MAGNETIC INTENSITY VARIATION ALONG THE LOWER WALL IN A UNIFORM DUCT WITH PERFECTLY CONDUCTING WALLS AS OBTAINED BY USING AN EXACT SOLUTION AND A FINITE ELEMENT SOLUTION FOR MODE 3 (TM_{30}) INCIDENT AT $z = 0$ WITH $\omega = 6.911$.

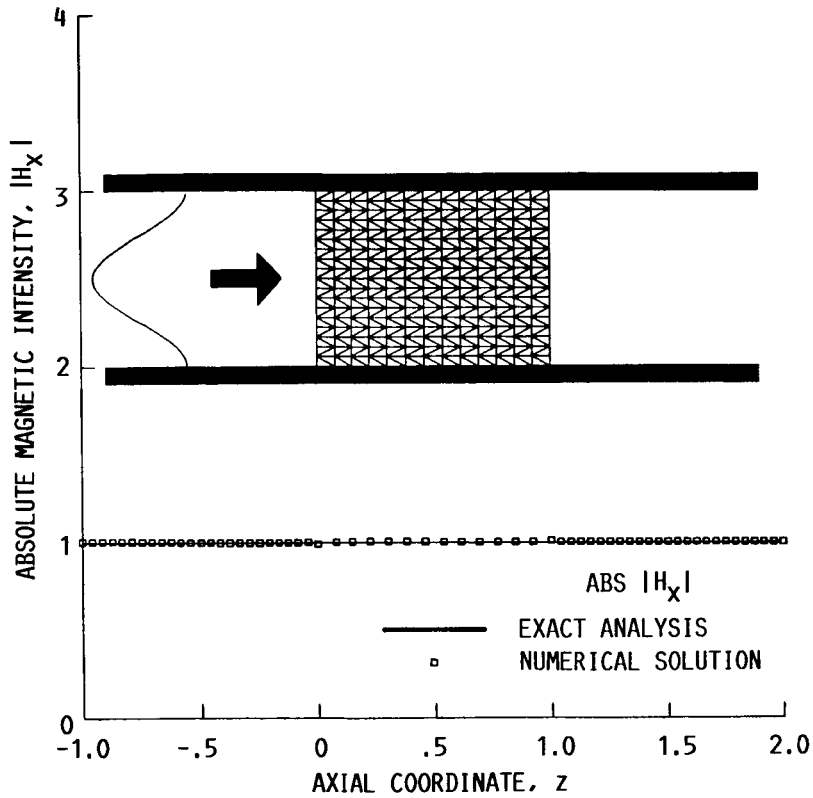


FIGURE 11.- A COMPARISON OF THE MAGNITUDE OF THE AXIAL MAGNETIC INTENSITY VARIATION ALONG THE LOWER WALL IN A UNIFORM DUCT WITH PERFECTLY CONDUCTING WALLS AS OBTAINED BY USING AN EXACT SOLUTION AND A FINITE ELEMENT SOLUTION FOR MODE-THREE INCIDENT (TM_{30}) AT $z = 0$ WITH $\omega = 6.911$.

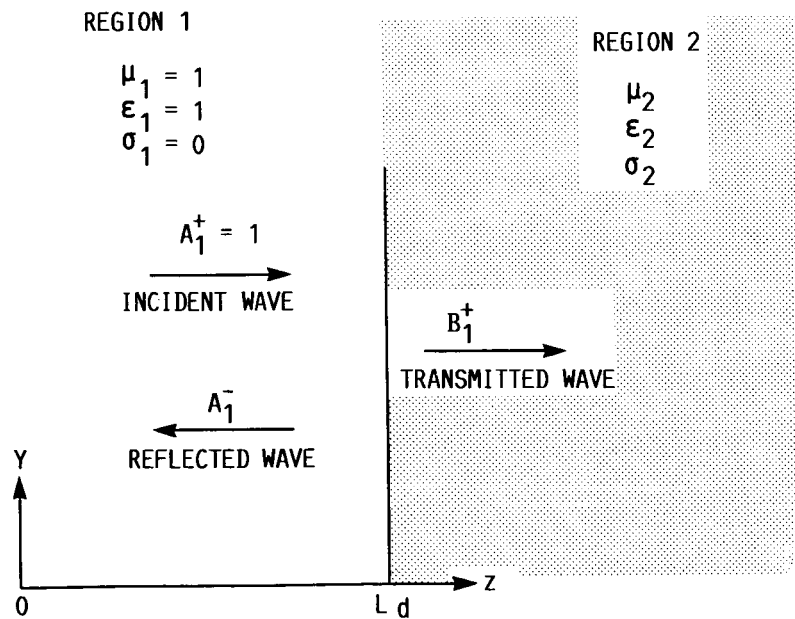


FIGURE 12.- A PLANE WAVE (TM_{10}) WITH NORMAL INCIDENCE ON A PLANE BOUNDARY.

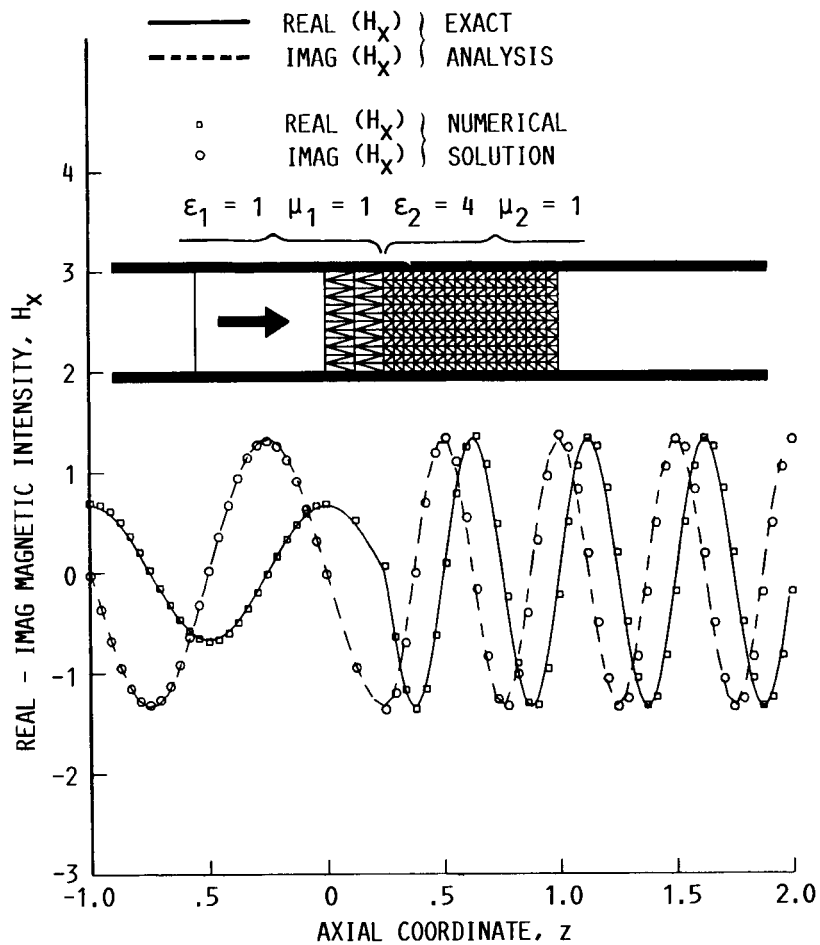


FIGURE 13. - A COMPARISON OF THE AXIAL MAGNETIC INTENSITY VARIATION ALONG THE LOWER WALL IN A UNIFORM DUCT WITH PERFECTLY CONDUCTING WALLS AND A CHANGE IN PROPERTIES OF THE MEDIA AT z OF 0.25 ($\epsilon_1 = 1.0$ AND $\epsilon_2 = 4.0$) AS OBTAINED BY USING AN EXACT SOLUTION AND A FINITE ELEMENT SOLUTION FOR A PLANE WAVE (MODE 1) INCIDENT AT $z = 0$ WITH $\omega = 2\pi$.

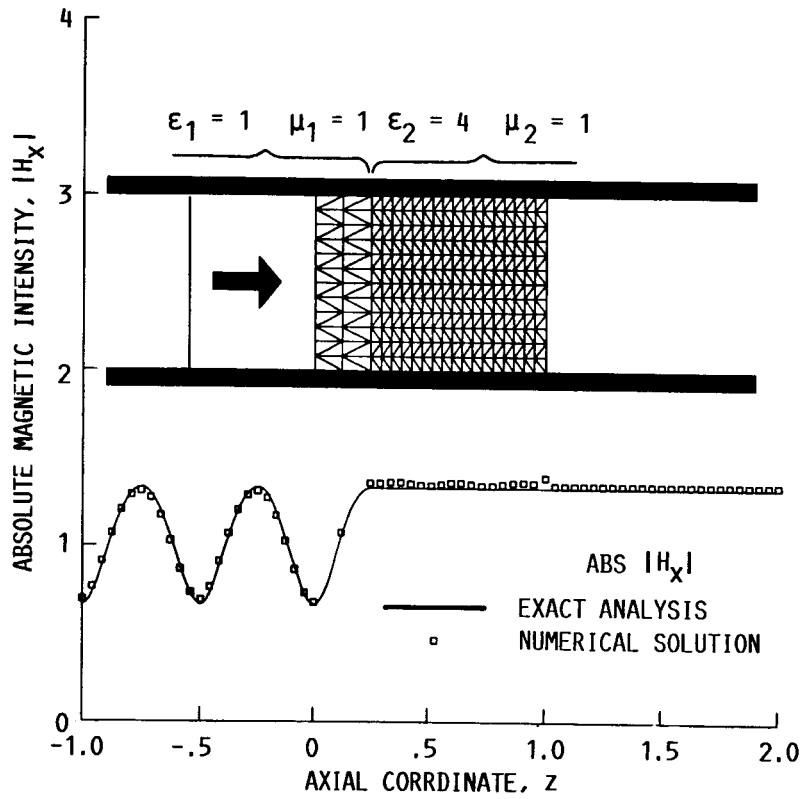


FIGURE 14. - A COMPARISON OF THE MAGNITUDE OF THE AXIAL MAGNETIC INTENSITY VARIATION ALONG THE LOWER WALL IN A UNIFORM DUCT WITH PERFECTLY CONDUCTING WALLS AND A CHANGE IN PROPERTIES OF THE MEDIA AT z OF 0.25 ($\epsilon_1 = 1.0$ AND $\epsilon_2 = 4.0$) AS OBTAINED BY USING AN EXACT SOLUTION AND A FINITE SOLUTION FOR A PLANE WAVE (MODE-ONE) INCIDENT AT $z = 0$ WITH $\omega = 2\pi$.

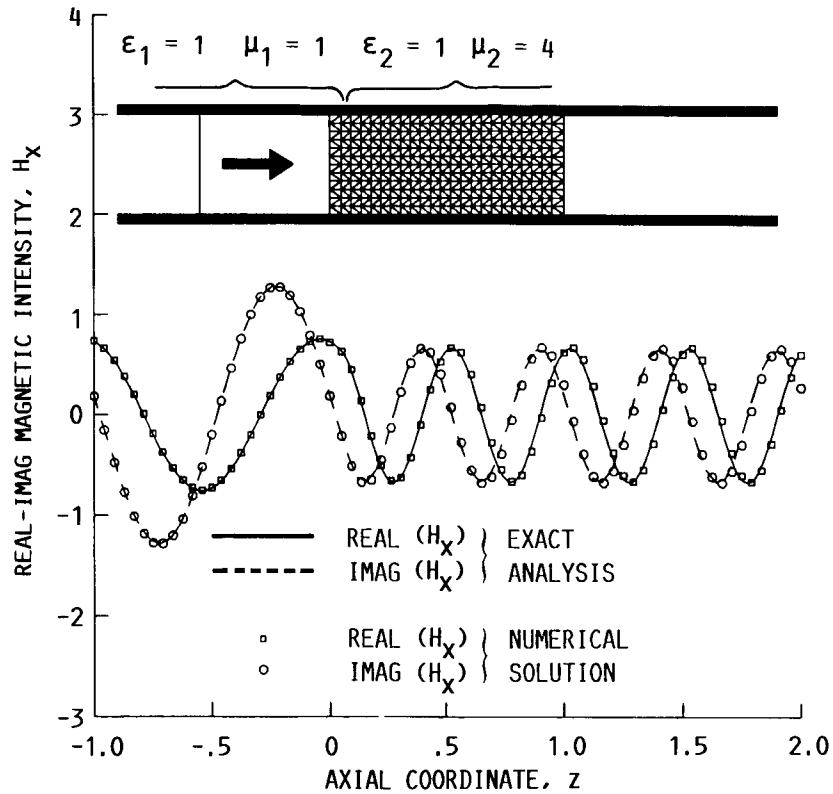


FIGURE 15.- A COMPARISON OF THE AXIAL MAGNETIC INTENSITY VARIATION ALONG THE LOWER WALL IN A UNIFORM DUCT WITH PERFECTLY CONDUCTING WALLS AND A CHANGE IN PROPERTIES OF THE MEDIA AT z OF 0.05 ($\mu_1 = 1.0$ AND $\mu_2 = 4.0$) AS OBTAINED BY USING AN EXACT SOLUTION AND A FINITE ELEMENT SOLUTION FOR A PLANE WAVE (MODE-ONE) INCIDENT AT $z = 0$ WITH $\omega = 2\pi$.

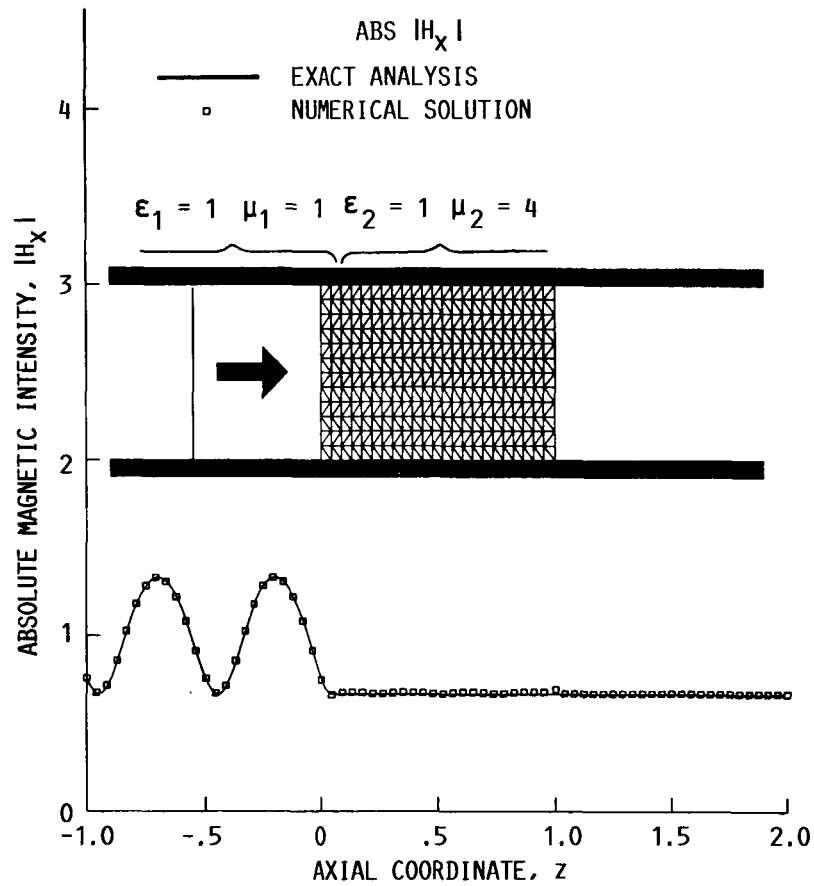


FIGURE 16.- A COMPARISON OF THE MAGNITUDE OF THE AXIAL MAGNETIC INTENSITY VARIATIONS ALONG THE LOWER WALL IN A UNIFORM DUCT WITH PERFECTLY CONDUCTING WALLS AND A CHANGE IN PROPERTIES OF THE MEDIA AT z OF 0.05 ($\mu_1 = 1.0$ AND $\mu_2 = 4.0$) AS OBTAINED BY USING AN EXACT SOLUTION AND A FINITE ELEMENT SOLUTION FOR A PLANE WAVE (MODE-ONE) INCIDENT AT $z = 0$ WITH $\omega = 2\pi$.

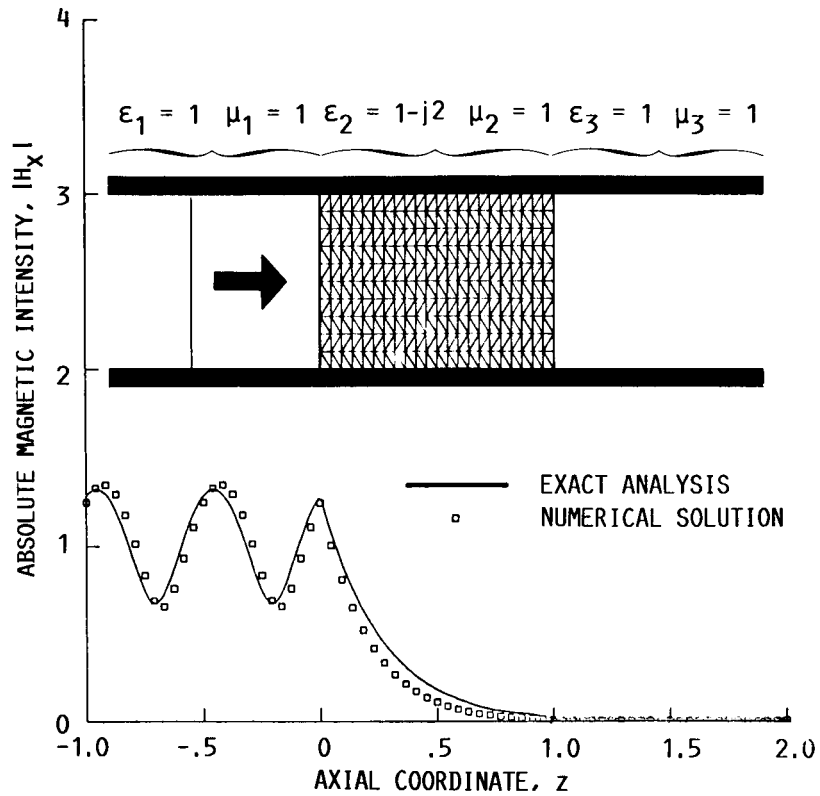


FIGURE 17. - A COMPARISON OF THE MAGNITUDE OF THE AXIAL MAGNETIC INTENSITY VARIATIONS ALONG THE LOWER WALL IN A UNIFORM DUCT WITH PERFECTLY CONDUCTING WALLS AND A CHANGE IN PROPERTIES OF THE MEDIA AT z OF 0.0 AS OBTAINED BY USING AN EXACT SOLUTION AND A FINITE ELEMENT SOLUTION FOR A PLANE WAVE (MODE-ONE) INCIDENT AT $z = 0$ WITH $\omega = 2\pi$.

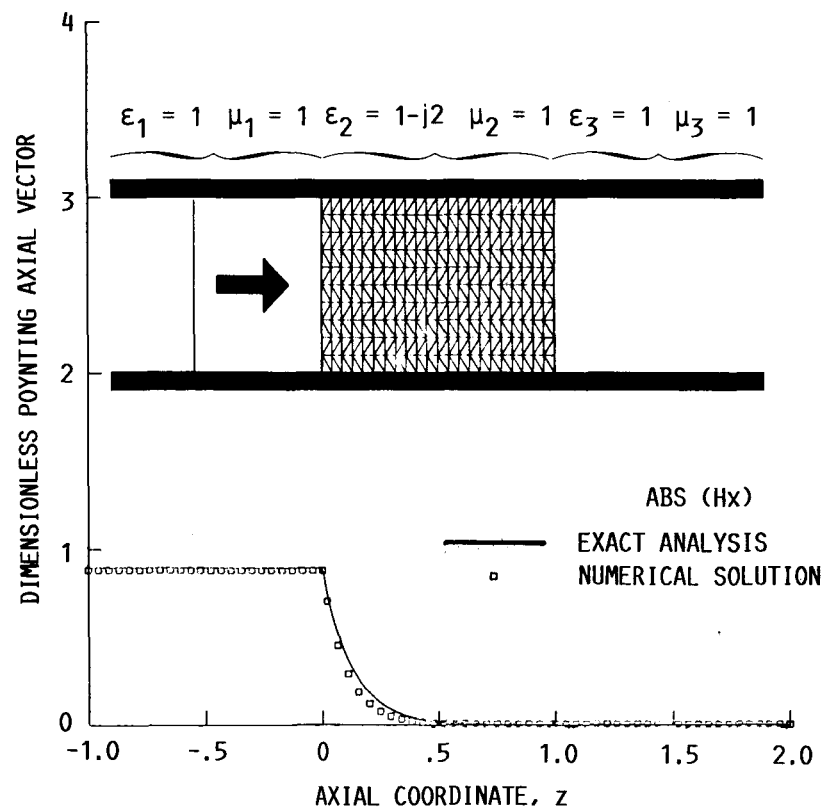


FIGURE 18. - A COMPARISON OF THE AXIAL FLUX OF ENERGY (POYNTING VECTOR) VARIATION IN A UNIFORM DUCT WITH PERFECTLY CONDUCTING WALLS AND A CHANGE IN PROPERTIES OF THE MEDIA AT z OF 0.0 AS OBTAINED BY USING AN EXACT SOLUTION AND A FINITE ELEMENT SOLUTION FOR A PLANE WAVE (MODE-ONE) INCIDENT AT $z = 0$.

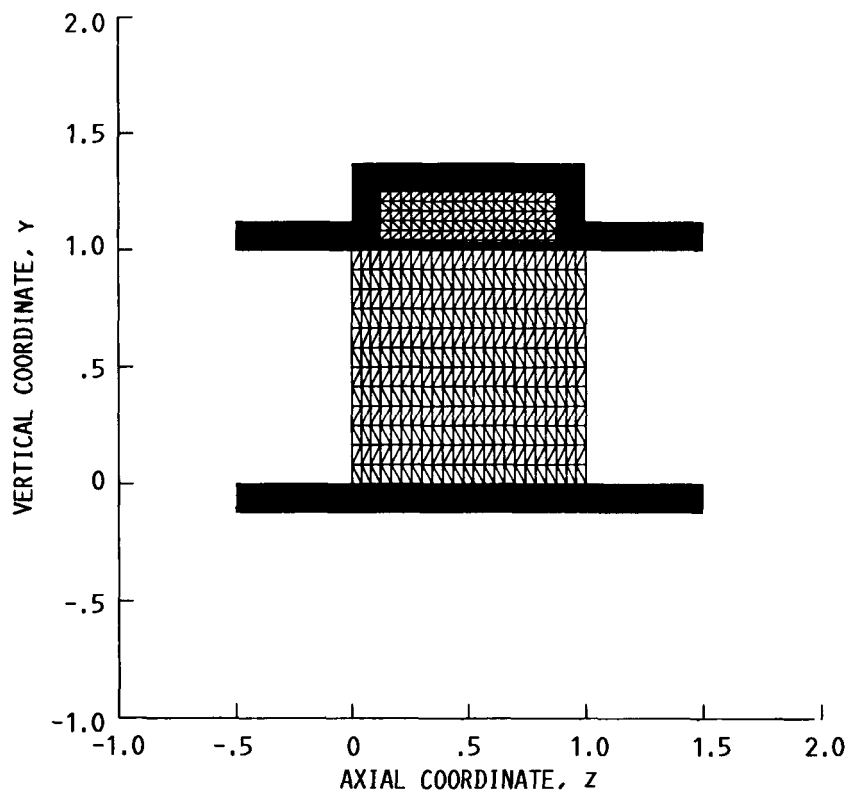


FIGURE 19.- DISCRETIZATION OF AIR FILLED WAVE GUIDE WITH ABSORBERS MOUNTED ALONG THE UPPER WALL.

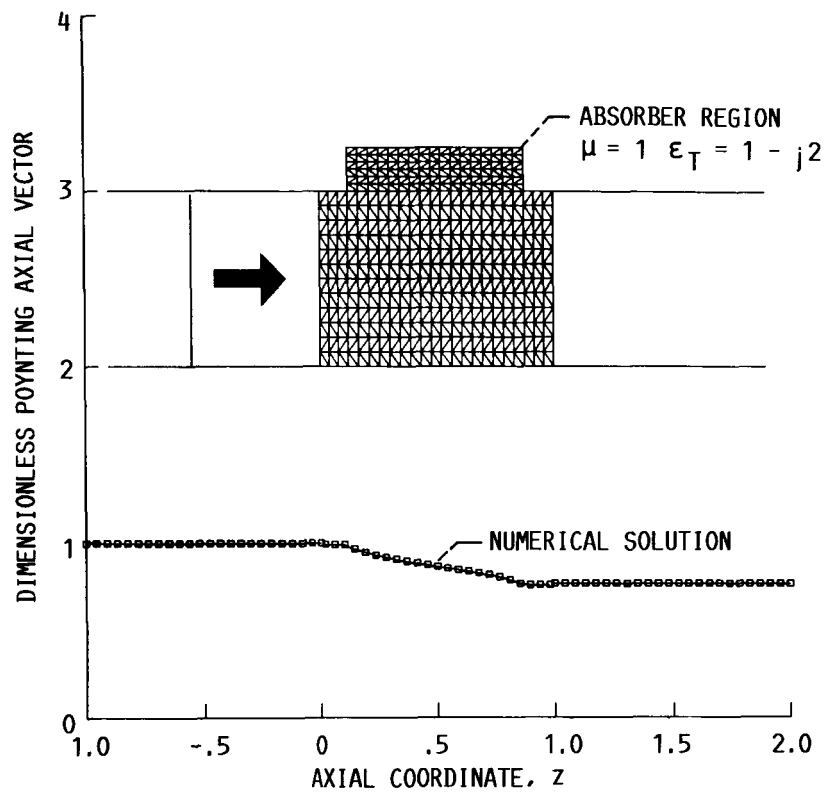


FIGURE 20.- EFFECT OF UPPER WALL ABSORBER ON THE MAGNITUDE OF THE AXIAL FLUX OF ENERGY (POYNTING VECTOR) FOR A THREE-MODE MODAL EXPANSION IN THE ENTRANCE AND EXIT DUCTS.

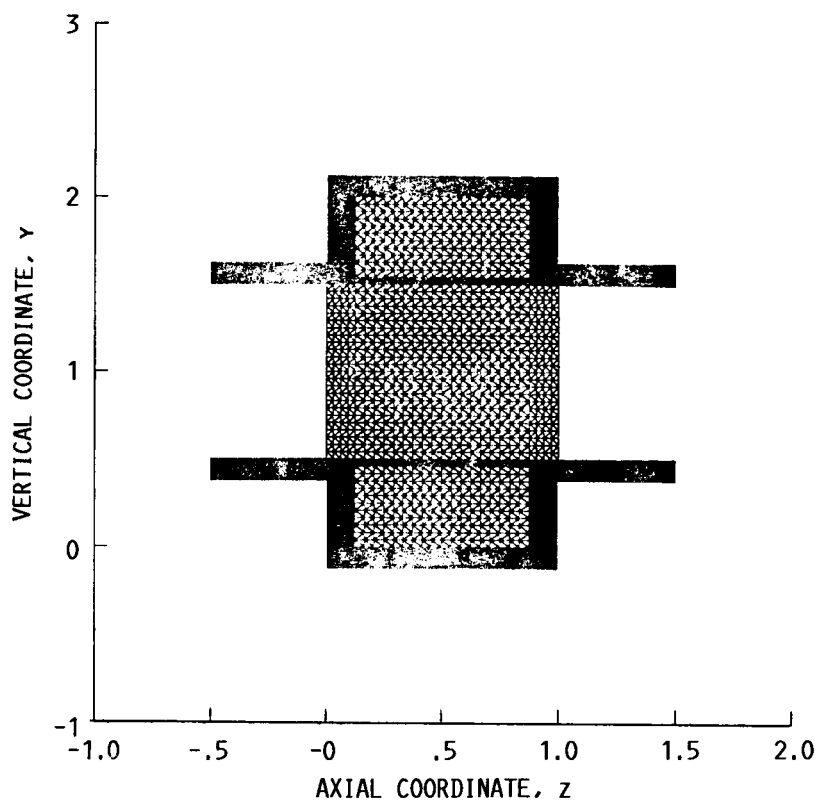


FIGURE 21.- DISCRETIZATION OF AIR FILLED WAVE GUIDE WITH ABSORBERS MOUNTED ALONG BOTH THE UPPER AND LOWER WALLS.

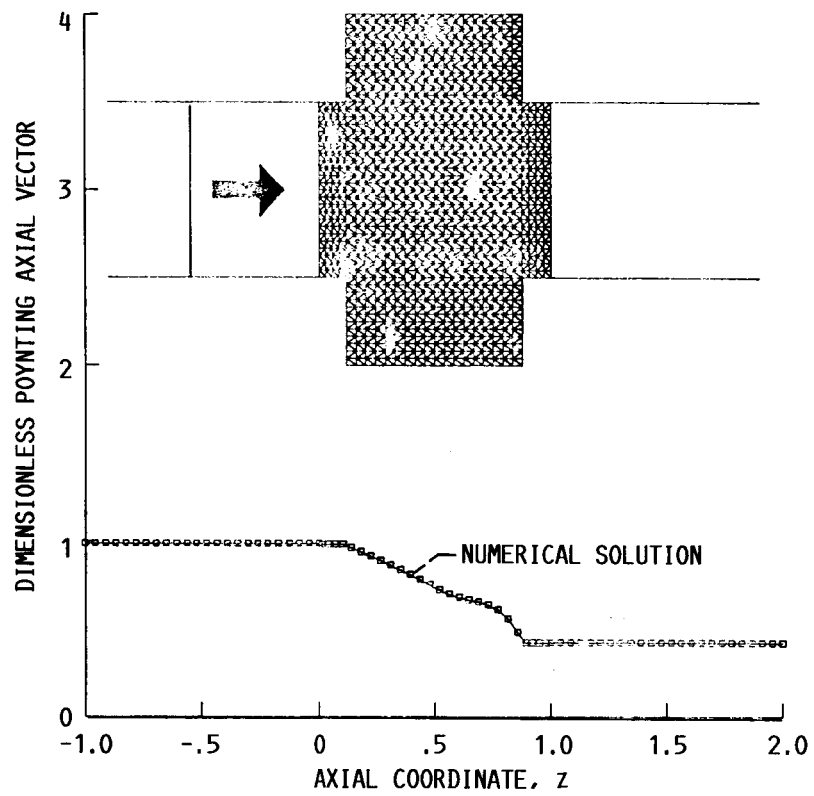
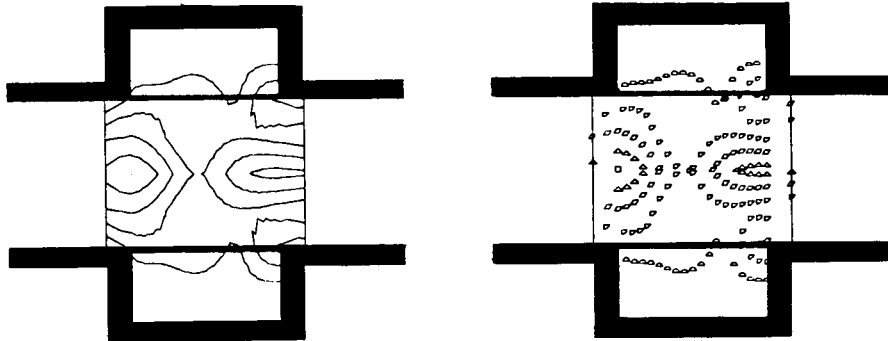


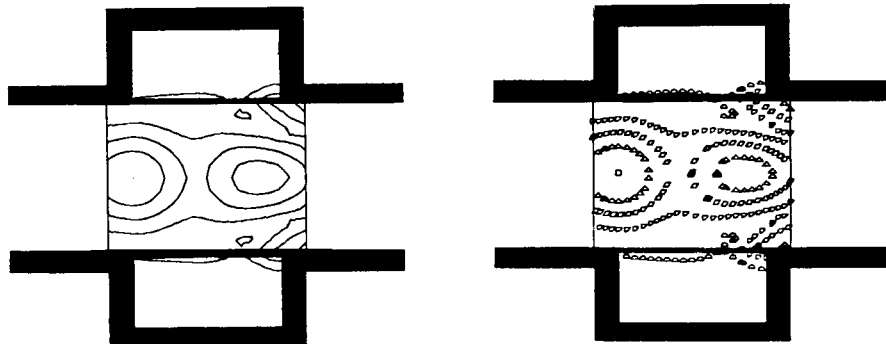
FIGURE 22.- EFFECT OF UPPER AND LOWER WALL ABSORBERS ON THE MAGNITUDE OF THE AXIAL FLUX OF ENERGY (POYNTING VECTOR) FOR A FIVE-MODE MODAL EXPANSION IN THE ENTRANCE AND EXIT DUCTS.

RELATIVE
MAGNITUDE

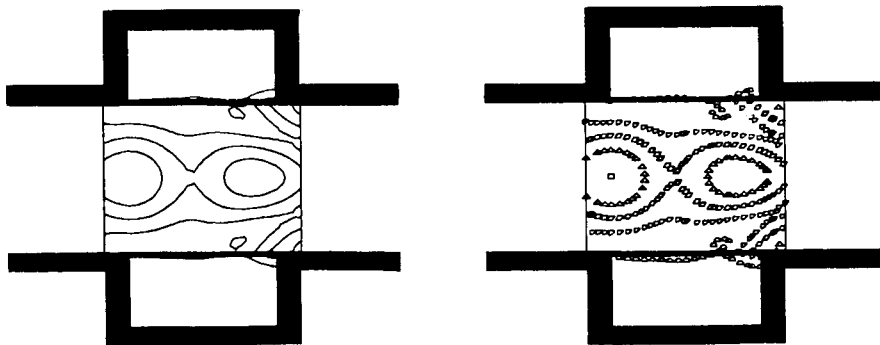
■ 1.0
▲ .8
◊ .6
◐ .4
◑ .2
○ 0



(A) 1 MODE MODAL EXPANSION.



(B) 3 MODES MODAL EXPANSION.



(C) 5 MODES MODAL EXPANSION.

FIGURE 23.- CONTOUR PLOTS OF MAGNETIC FIELD AMPLITUDE.

44	64	84	104	124
43	63	83	103	123
42	62	82	102	122
41	61	81	101	121
40	60	80	100	120
39	59	79	99	119
38	58	78	98	118
37	57	77	97	117

ELEMENT NUMBERS UPPER SOFT REGION

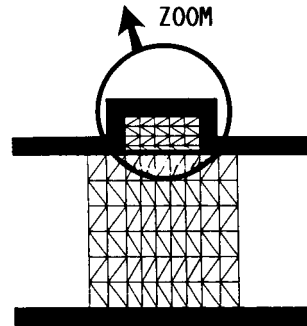


FIGURE 24.- ZOOM CAPABILITIES OF FINITE ELEMENT CODE.

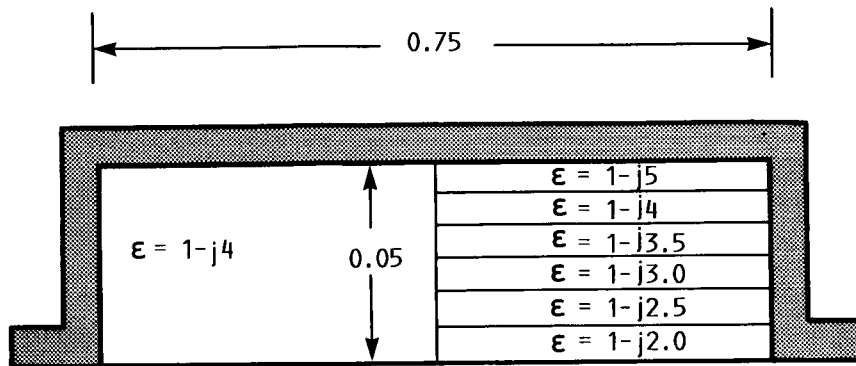


FIGURE 25.- MULTIPLE THIN FILM WALL ABSORBER CONFIGURATION (NOT TO SCALE).

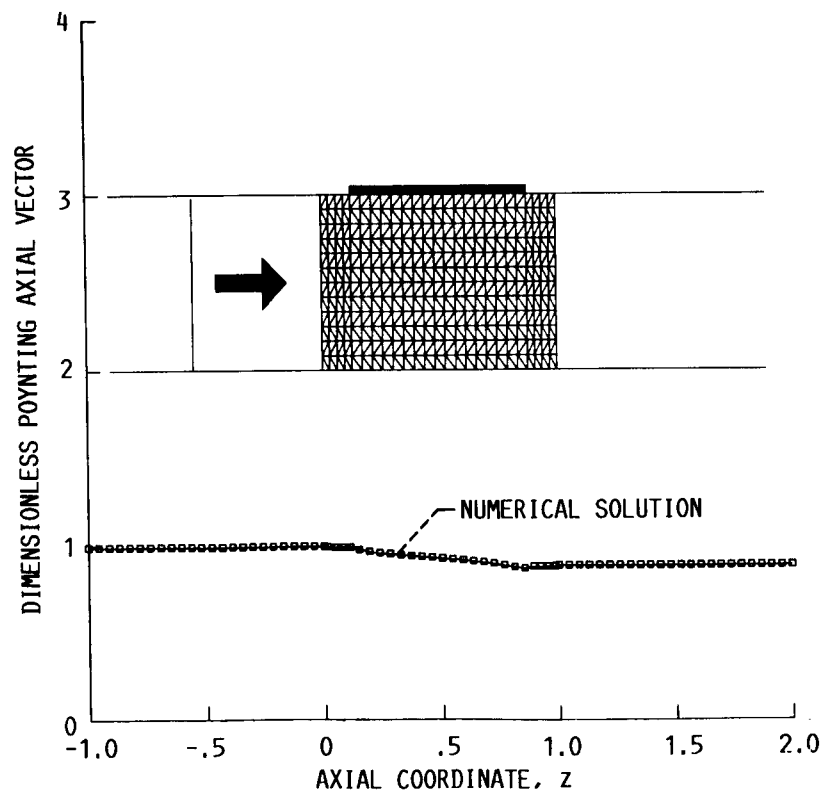


FIGURE 26.- EFFECT OF MULTIPLE THIN FILM WALL ABSORBER ON THE MAGNITUDE OF THE AXIAL FLUX OF ENERGY (POYNTING VECTOR).

1. Report No. NASA TM-88866		2. Government Accession No.		3. Recipient's Catalog No.	
4. Title and Subtitle Finite Element Analysis of Electromagnetic Propagation in an Absorbing Wave Guide				5. Report Date	
				6. Performing Organization Code 505-62-21	
7. Author(s) Kenneth J. Baumeister				8. Performing Organization Report No. E-3133	
				10. Work Unit No.	
9. Performing Organization Name and Address National Aeronautics and Space Administration Lewis Research Center Cleveland, Ohio 44135				11. Contract or Grant No.	
				13. Type of Report and Period Covered Technical Memorandum	
12. Sponsoring Agency Name and Address National Aeronautics and Space Administration Washington, D.C. 20546				14. Sponsoring Agency Code	
15. Supplementary Notes Prepared for the 1986 Winter Annual Meeting of the American Society of Mechanical Engineers, Anaheim, California, December 7-12, 1986.					
16. Abstract Wave guides play a significant role in microwave space communication systems. The attenuation per unit length of the guide depends on its construction and design frequency range. A finite element Galerkin formulation has been developed to study TM electromagnetic propagation in complex two-dimensional absorbing wave guides. The analysis models the electromagnetic absorptive characteristics of a general wave guide which could be used to determine wall losses or simulate resistive terminations fitted into the ends of a guide. It is believed that the general conclusions drawn by using this simpler two-dimensional geometry will be fundamentally the same for other geometries.					
17. Key Words (Suggested by Author(s)) Finite element; Electromagnetic waves; Duct propagation; Absorption			18. Distribution Statement Unclassified - unlimited STAR Category 70		
19. Security Classif. (of this report) Unclassified		20. Security Classif. (of this page) Unclassified		21. No. of pages	22. Price*